AD-A049 540 STANFORD UNIV CALIF EDWARD L GINZTON LAB F/G 20/5
OPTICALLY PUMPED MERCURY LASERS FOR RING LASER GYROSCOPE APPLIC--ETC(U)
OCT 77 N C HOLMES, A E SIEGMAN AFOSR-76-3043

UNCLASSIFIED GL-2736 AFOSR-TR-78-0023 NL

| OF |
AD
A049540

END
DATE
FILMED
3-78
DDC

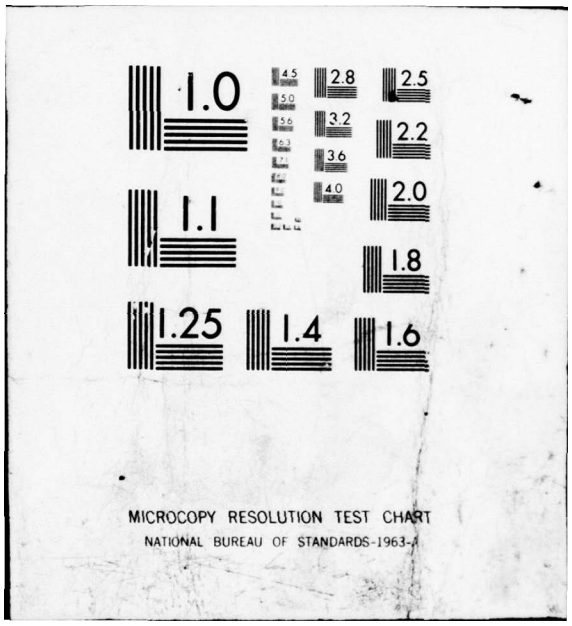
1.0
1.1
1.25
1.4
1.6
1.8
2.0
2.2
2.5
2.8
3.2
3.6
4.0
4.5
5.0
5.6
6.3
MICROCOPY RESOLUTION TEST CHART
NATIONAL BUREAU OF STANDARDS-1963-A

AFOSR-TR- 78-0023

(2)
B.S.

OPTICALLY PUMPED MERCURY LASERS FOR RING LASER GYROSCOPE APPLICATIONS

Final Technical Report

for

Grant AFOSR 76-3043

Prepared for

Department of the Air Force

Air Force Office of Scientific Research

Bolling Air Force Base, DC 20332

for the period

1 June 1976 – 31 August 1977

G. L. Report No. 2736

October 1977

Principal Investigator

Professor A. E. Siegman
Department of Electrical Engineering

Edward L. Ginzton Laboratory
W. W. Hansen Laboratories of Physics
Stanford University
Stanford, California

UNCLASSIFIED

SECURITY CLASSIFICATION OF THIS PAGE (When Data Entered)

(19) REPORT DOCUMENTATION PAGE

READ INSTRUCTIONS BEFORE COMPLETING FORM

1. REPORT NUMBER: (18) AFOSR TR-78-0023 ✓
2. GOVT ACCESSION NO.
3. RECIPIENT'S CATALOG NUMBER

4. TITLE (and Subtitle): (6) OPTICALLY PUMPED MERCURY LASERS FOR RING LASER GYROSCOPE APPLICATIONS
5. TYPE OF REPORT & PERIOD COVERED: (9) FINAL technical rept. 1 Jun [redacted] 76 - 31 Aug [redacted] 77
6. PERFORMING ORG. REPORT NUMBER: (14) GL-2736

7. AUTHOR(s): (10) N. C. Holmes [redacted] A. E. Siegman
8. CONTRACT OR GRANT NUMBER(s): (15) AFOSR-76-3043 ✓ new

9. PERFORMING ORGANIZATION NAME AND ADDRESS
Stanford University
Department of Electrical Engineering ✓
Stanford, California 94305
10. PROGRAM ELEMENT, PROJECT, TASK AREA & WORK UNIT NUMBERS: (16) 61102F, (17) 2305 B2

11. CONTROLLING OFFICE NAME AND ADDRESS
Director of Electronics and Solid State Sciences
Air Force Office of Scientific Research
Bolling AFB Building 410, Washington, D.C. 20332
12. REPORT DATE: (11) Oct [redacted] 1977
13. NUMBER OF PAGES: 78 (12) 79p.

14. MONITORING AGENCY NAME & ADDRESS (if different from Controlling Office)
15. SECURITY CLASS. (of this report): UNCLASSIFIED
15a. DECLASSIFICATION/DOWNGRADING SCHEDULE

16. DISTRIBUTION STATEMENT (of this Report)

Approved for Publication Release: Distribution Unlimited

17. DISTRIBUTION STATEMENT (of the abstract entered in Block 20, if different from Report)

18. SUPPLEMENTARY NOTES

19. KEY WORDS (Continue on reverse side if necessary and identify by block number)

Lasers
Laser mode-locking
Laser gyroscope
Metal vapor lasers
Mercury laser
Hg laser
Optically pumped laser

20. ABSTRACT (Continue on reverse side if necessary and identify by block number)

In this investigation, both the theoretical and practical aspects of the optically pumped cw mercury vapor laser at 546.1 nm have been explored. A rate-equation analysis was used to develop a quantitative model describing the nitrogen pressure dependence of laser power output and unsaturated gain. Careful measurements show the model to be in excellent agreement with experiment. Measurements were also made as the pumping rates, bore diameter, and mercury

(continue on back page)

DD FORM 1 JAN 73 1473 EDITION OF 1 NOV 65 IS OBSOLETE

[redacted] 409 640 JOB

density were varied. A qualitative treatment of the effects of high intensity pumping and radiation trapping is given, and this analysis is consistent with the observed behavior.

The nitrogen quenching rate across the laser transition was found to be $7 \cdot 10^5$ sec^{-1}-$Torr^{-1}$, and the pressure broadening of the green laser line was inferred to be 26.4 MHz/Torr.

A detailed description of the experimental apparatus is given. Together with the experimental measurements, this work can provide a basis for the design of practical mercury laser systems.

ABSTRACT

In this investigation, both the theoretical and practical aspects of the optically pumped cw mercury vapor laser at 546.1 nm have been explored. A rate-equation analysis was used to develop a quantitative model describing the nitrogen pressure dependence of laser power output and unsaturated gain. Careful measurements show the model to be in excellent agreement with experiment. Measurements were also made as the pumping rates, bore diameter, and mercury density were varied. A qualitative treatment of the effects of high intensity pumping and radiation trapping is given, and this analysis is consistent with the observed behavior.

The nitrogen quenching rate across the laser transition was found to be $7 \cdot 10^5$ sec^{-1}-$Torr^{-1}$, and the pressure broadening of the green laser line was inferred to be 26.4 MHz/Torr.

A detailed description of the experimental apparatus is given. Together with the experimental measurements, this work can provide a basis for the design of practical mercury laser systems.

700,000 per sec per Torr

TABLE OF CONTENTS

LIST OF FIGURES

CHAPTER I

THEORY

A. INTRODUCTION

The behavior of optically pumped mixtures of mercury and nitrogen has been studied for more than 50 years. The enhancement of the green fluorescence of mercury at 546.1 nm in the presence of nitrogen was under investigation by Wood[1] as early as 1925. Over the years, many attempts to model the Hg-N_2 system have been proposed.[2-5] Today, the physical processes are reasonably well understood, and many of the important rate constants have been measured. The use of Hg-N_2 mixtures in photochemistry, optical pumping, and sensitized fluorescence provided the major impetus for this earlier work.

Interest in the Hg-N_2 system increased recently, following the report in 1974 by Djeu and Burnham[6] of cw laser action on the 546.1 nm mercury line in optically pumped Hg-N_2 mixtures. Motivated by several potential applications for this laser, we have conducted both experimental and theoretical studies of the Hg-N_2 laser system. In Chapter I we present a model of laser operation. The results of experimental measurements are given in Chapter II, and compared with the predictions of the model.

Following earlier workers, we use a steady-state rate equation analysis to develop a model for the gain and saturation properties of this

system. The behavior of both the laser output power and the gain, especially as a function of nitrogen pressure, can then be explained. The effects of mercury density, pumping rates and laser tube diameter have also been considered, but the analysis of these effects is much more difficult and only a simplified treatment will be given here.

B. RATE EQUATIONS

Before writing down the rate equations, a brief review of the Hg laser operation may be in order. The important energy levels for the mercury laser are shown in Fig. 1. The laser is typically operated in a transparent fused silica tube 4 mm in diameter, containing a mixture of mercury at a density of 10^{14} cm^{-3}, and nitrogen at a pressure of 35 Torr. This mixture is optically excited by high intensity mercury pump lamps. The Hg resonance line at 253.7 nm from the pump lamp is absorbed by the ground $^1S_0$ level Hg atoms, strongly populating the $^3P_1$ level. While in this state the mercury atoms undergo a large number of Hg-N_2 collisions. These collisions quench the atoms in $^3P_1$ to the metastable $^3P_0$ level by transferring energy to the first vibrationally excited state of the nitrogen molecules. If the pumping is sufficiently intense, a high density of $^3P_0$ atoms is formed.

These atoms can then absorb pump light at 404.7 nm, populating the $^3S_1$ upper laser level. Nearly resonant inelastic collisions of the Hg atoms in the $^3P_2$ level with nitrogen molecules also rapidly quench the $^3P_2$ level. At nitrogen pressures greater than ~ 10 Torr, this quenching of the $^3P_2$ level becomes rapid enough to establish conditions for laser

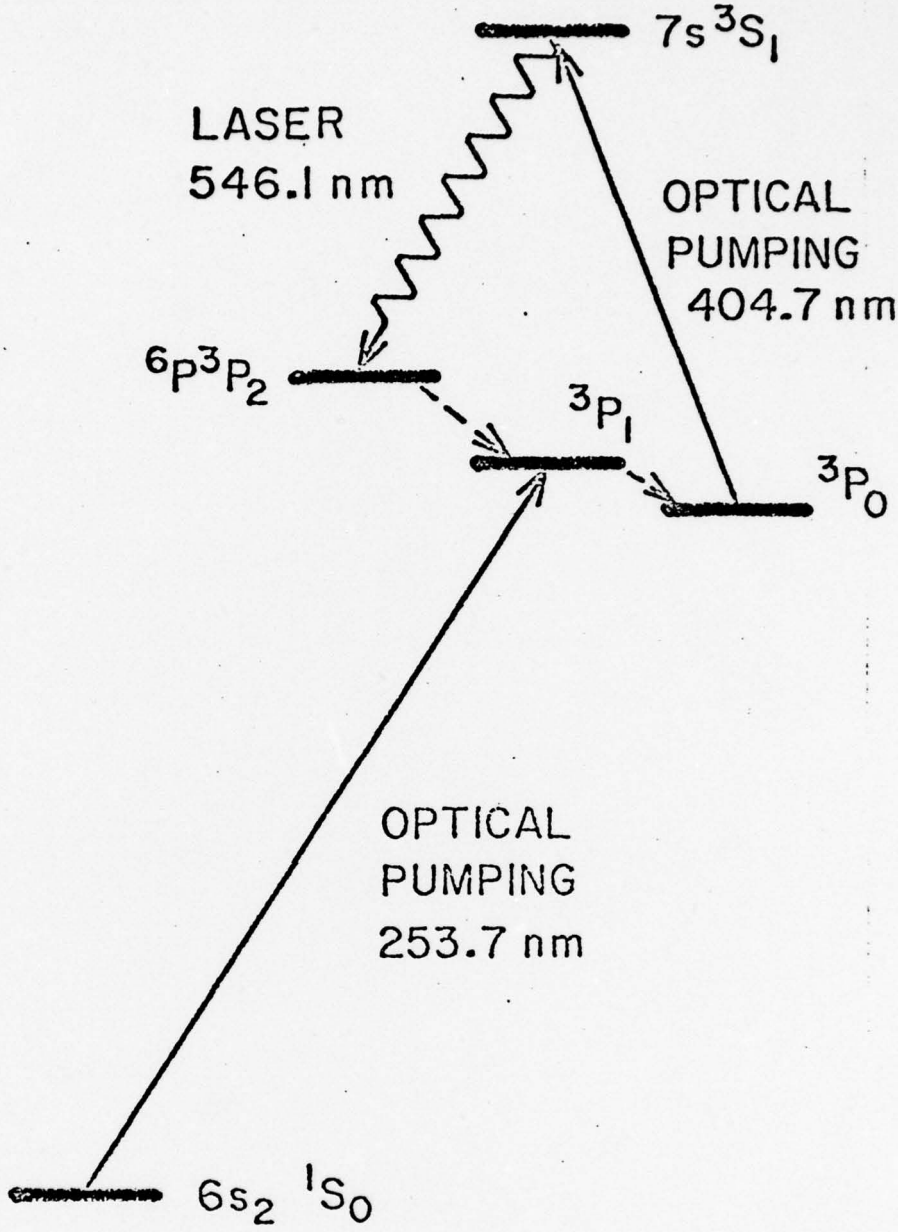

FIG. 1--Mercury energy levels and optical pumping scheme.

gain and cw laser oscillation on the green 546.1 nm mercury transition between $^3S_1$ and $^3P_2$.

In Figure 2, the relevant processes in the Hg laser are shown schematically, with various transition rates as defined below. The population densities in the mercury levels are denoted as: $N_0 = [^1S_0]$, $N_1 = [^3P_0]$, $N_2 = [^3P_1]$, $N_3 = [^3P_2]$, $N_4 = [^3S_1]$. We can then write the rate equations viz:

$$\dot{N}_0 = - R_0 N_0 + (A_{20} + K_{20}) N_2 + K_{10} N_1 \tag{1}$$

$$\dot{N}_1 = K_{21} N_2 + (A_{41} + K_{41}) N_4 - (R_p + K_{10} + K_{12}) N_1 + D\nabla^2 N_1 \tag{2}$$

$$\dot{N}_2 = R_0 N_0 - (A_{20} + K_{20} + K_{21}) N_2 + K_3 N_3 + K_{12} N_1 + (A_{42} + K_{42}) N_4 \tag{3}$$

$$\dot{N}_3 = W_{43} (N_4 - g_4/g_3 \, N_3) + (A_{43} + K_{43}) N_4 - K_3 N_3 \tag{4}$$

$$\dot{N}_4 = - W_{43} (N_4 - g_4/g_3 \, N_3) - (A_4 + K_4) N_4 + R_p N_1 \tag{5}$$

$$N = N_0 + N_1 + N_2 + N_3 + N_4 \tag{6}$$

where

R_0 = Pumping rate due to 253.7 nm absorption.

R_p = Pumping rate due to 404.7 nm absorption.

A_{ij} = Spontaneous radiative decay rate from state i to state j .

K_{ij} = Non-radiative (quenching) decay rate from state i to state j .

K_{10} = Total decay rate of $^3P_0$ due to quenching, radiative decay, molecule or ion formation, etc.

W_{43} = Stimulated emission rate between $^3S_1$ and $^3P_2$.

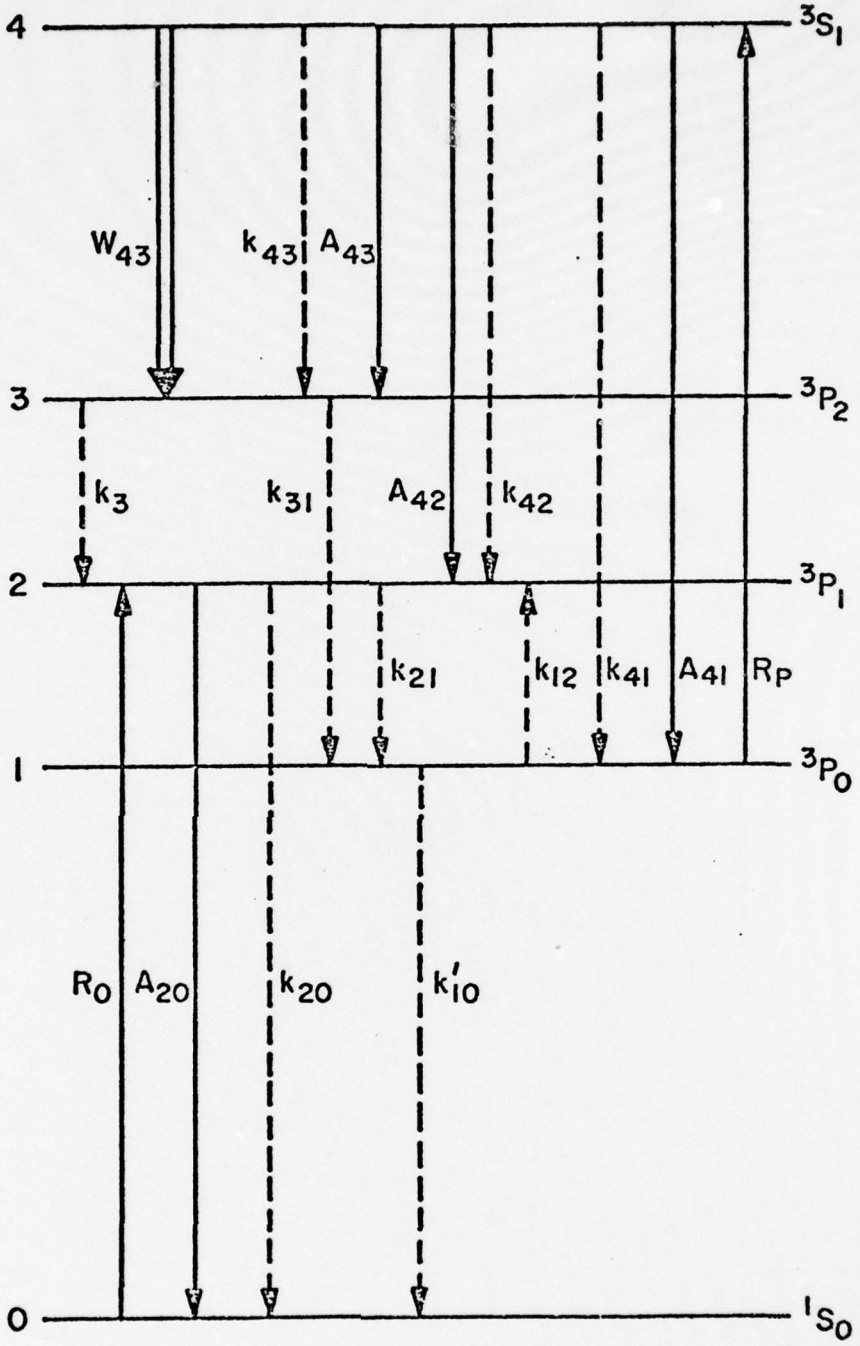

FIG. 2--Detailed energy level diagram of mercury. Solid lines indicate optical processes, dashed lines indicate non-radiative (quenching) processes.

A_i, K_i = Total radiative or quenching rates out of state i .

D = Diffusion coefficient for Hg atoms in N_2 .

N = Total density of Hg atoms.

g_4, g_3 = Dengeneracies of upper and lower laser levels.

Best estimates of the numerical values for these parameters are summaried in Table I.

In general, the population densities N_i and the pumping rates R_0 and R_p are functions of position in the laser medium, so that Eqs. (1-5) are strictly valid only over volume elements sufficiently small that the pumping rates and population densities are constant. However, we will show that these equations in a "volume-averaged" form do actually give an accurate account of laser operation.

This spatial dependence of the level population densities is involved explicity in Eq. (2) through the diffusion term involving $\nabla^2 N_1$. It is possible to expand the spatial dependence of each of the densities N_i in terms of the eigenfunctions of the diffusion equation. The boundary conditions to be satisfied are, first that the excited state populations should be zero at the tube walls, since all excited atoms that hit them are quenched to ground. Second, since the problem is axially symmetric, we expect that the population densities should have a zero radial derivative at the center of the tube. The eigenfunctions of the diffusion equation for a long cylinder that satisfy these boundary conditions are the J_0 Bessel functions. Thus we can write

$$N_i(r) = \sum_{k=1}^{\infty} a_{ik} J_0\left(\frac{z_k}{R} r\right)$$

where the a_{ik} are expansion coefficients, R is the tube radius, and

TABLE I

MERCURY LASER RATES

Radiative Rates	Value (sec^{-1})	Estimated Relative Error	Reference
A_{20}	$8.3 \cdot 10^6$	1%	12
A_{43}	$4.5 \cdot 10^7$	3%	16
A_{42}	$4.2 \cdot 10^7$	3%	16
A_{41}	$1.6 \cdot 10^7$	3%	16
Quenching Rates at 1 Torr Nitrogen, 320° K	**Value (sec^{-1})**	**Estimated Relative Error**	**Reference**
K_{21}	$1.14 \cdot 10^5$	10%	13
K_{12}	67	10%	13
K_{20}	< 630	3%	13
t	≤ 1	3%	13
K_4	$4.4 \cdot 10^6$	5%	14
K_3	$3.0 \cdot 10^6$	35%	15
K_{43}	$7 \cdot 10^5$	50%	This work
Decay rate of $^3P_0$ at $[Hg] = 10^{14}\ cm^{-3}$			
K	$1.8 \cdot 10^4\ sec^{-1}$	±50%	17
Diffusion constant, at 1 Torr nitrogen			
D	124 cm^2/sec	±20%	7

z_k is the k-th zero of J_0 . To evaluate the coefficients a_{ik} for any specific case, the spatial dependence of the pumping must be known. This is not easily determined, as we will show later. The loss rate for the k-th Bessel mode is $a_{ik}\, D(z_k/R)^2$. Thus, higher order modes will have much higher diffusion losses. In many cases keeping only the lowest-order Bessel mode is an adequate approximation. Calculations of the radial populations $N_i(r)$ for the Hg laser have been performed under the simplifying assumption that the pumping rate at 253.7 nm is not sufficiently intense to deplete the ground level populations. These calculations show that for a wide range of conditions the first term in the expansion is dominant. If for simplicity only the first term is used in calculating the diffusion losses for the $^3P_0$ level then the $D\nabla^2 N_1$ term in Eq. (2) is replaced in the rate equations by

$$D\nabla^2 N_1 \approx - D \left(\frac{2.405}{R}\right)^2 N_1 = - D_0 N_1$$

Using the value of D in Table I gives $D_0 = 1.8 \cdot 10^4$ sec^{-1}-Torr for a 4 mm diameter laser tube. If the pumping conditions are such that N_1 departs from the assumed J_0 distribution, then the diffusion loss rate can be expected to be somewhat higher. All the excited states other than $^3P_0$ have such short lifetimes that diffusion can be safely neglected in their rate equations.

Some additional simplifications have been made as well. Backward quenching rates such as K_{23} , K_{14} , etc. have not been included because they are expected to be negligible, as shown by detailed balancing arguments. Also, some possible but unknown quenching processes such as $^3S_1$ directly to $^1S_0$ have not been included.

The formal solutions to Eqs. (1)-(6) for the small-signal case $W_{43} = 0$ and for steady-state operation may be written as

$$N_0 = N[K'_{10}K_{21}K_3 f + aK_3(bf - R_p c)]/\Delta \tag{7}$$

$$N_1 = NR_0K_{21}K_3 f/\Delta \tag{8}$$

$$N_2 = NR_0K_3(bf - R_p c)/\Delta \tag{9}$$

$$N_3 = NR_0R_pK_{21}d/\Delta \tag{10}$$

$$N_4 = NR_0R_pK_{21}K_3/\Delta \tag{11}$$

where

$$\Delta = K_3[R_0 f(b + K_{21}) + f(K'_{10}K_{21} + ab) - acR_p] + R_0R_p(K_3K_{21} + K_{21}d - K_3c)$$

$$a = A_{20} + K_{20} + D_0 \qquad d = A_{43} + K_{43}$$

$$b = R_p + K'_{10} + K_{12} \qquad f = A_4 + K_4$$

$$c = A_{41} + K_{41} \qquad K'_{10} = K_{10} + D_0$$

While this form is useful for calculation, the nitrogen pressure dependence of the population densities is unclear. To make the pressure dependence explicit, we let $K_{ij} = t_{ij}P$ where P is the nitrogen pressure. Further, let $K'_{10} = K + tP + d_0/P$ since D_0 is inversely proportional to pressure.

As an aside, consider the case of the three-level optically pumped system using only the three levels $^1S_0$, $^3P_0$, $^3P_1$. This is equivalent

to setting $R_p = 0$ in the above solutions. Since $R_0 \ll A_{20}$ in most cases of interest, we can write

$$N_1(P) = N \frac{R_0 t_{21} P^2}{A_{20} d_0} \left\{ \frac{t_{21} t + t_{20} t_{12} + t_{20} t}{A_{20} d_0} P^3 + \frac{R_0(t_{12} + t_{21} + t) + t_{21} K + A_{20}(t_{12} + t) + t_{20} K}{A_{20} d_0} P^2 + \left(\frac{K}{d_0} + \frac{t_{21} + t_{20}}{A_{20}} \right) P + 1 \right\}^{-1} \tag{12}$$

This is similar in form to several well-known earlier expressions including those of Gaviola,[3] Kimbell and Leroy,[7] and for $d_0 = 0$ that used by Berberet and Clark[8] based on work by Klumb and Pringsheim.[5] Note that N_1 is roughly proportional to R_0 for weak pumping and falls, although slowly, as $1/P$ for large P. This behavior is confirmed by other workers.[7,8] We attempted to confirm this behavior experimentally in our laser tube using the absorption of the 404.7 nm line as a probe. Unfortunately, the strong pressure broadening of this blue line[9] prevented this.

There is an additional complication which should be noted at this time. The $^3P_0$ quenching rate K in the above expressions has been found to be proportional to the ground level mercury density. If the pumping rate R_0 is sufficiently great, the $^1S_0$ level may become somewhat depleted, and this will reduce the rate K. Since K is a "lumped" rate containing all the nitrogen pressure-independent rates, it also has contributions from Hg molecule and Hg ion formation.

These effects may become important when N_1 is large. Thus, some caution is advised in the use of these expressions.

To evaluate the unsaturated gain, two paths may be taken. The most obvious is to make direct use of Eqs. (10) and (11). The unsaturated gain g_0 is then given by

$$g_0 = (N_4 - g_4/g_3 N_3)\,\sigma^2(P) \tag{13}$$

where $\sigma^2(P)$ is the atomic transition cross section. This cross-section is probably pressure dependent due to the broadening and shift of the laser line which is to be expected at the relatively high nitrogen pressures used in typical operation. Substituting for N_3 and N_4 then gives

$$g_0 = NR_0R_pK_{21}\sigma^2(P)(K_3 - g_4/g_3\, d)/\Delta \tag{14}$$

Alternatively, if we have knowledge of the metastable population density N_1, the gain can be expressed as

$$g_0 = \frac{R_p N_1(P)}{f}\,\sigma^2(P)\left(1 - \frac{g_4}{g_3}\frac{d}{K_3}\right) \tag{15}$$

The functional form of the variation of gain with pressure is then

$$g_0 \propto \frac{\alpha P^2 - \beta P}{\gamma P^4 + \delta P^3 + \epsilon P^2 + \zeta P + 1}\,\sigma^2(P) \tag{16}$$

This shows that the gain should fall as $1/P^2$ for the large P, and that a threshold is expected for $P = \beta/\alpha$. This expression is not a particularly useful form for computational purposes, but is used in Chapter II as a model for curve-fitting of experimental gain data.

Typical Solution of the Rate Equations

For these solutions to be useful for design calculations, we must have good estimates of the pumping rates, and accurate values for the rate constants. The important rates useful for this purpose are given in Table I. It should be emphasized that the uncertainties for some of these rates are large. Indeed, a thorough study of the literature discloses that there are often much larger variations from experiment to experiment than even these errors imply. Thus, any numerical calculation based on these rates should be viewed with some skepticism. As more reliable rate coefficients become available, the predictive ability of our analysis will be enhanced.

The evaluation of the pumping rates is also not simple. These will be discussed at some length in a subsequent section. For now, we will employ a simple estimate. We will assume that the laser tube is uniformly illuminated by the lamp(s), and that the pump rates for both lines are constant throughout the laser tube. If V is the volume of the tube, and ν the frequency of the pump radiation, the power absorbed is given by $P_{ABS} = RNh\nu V$, where R is the pump rate, and N is the density of the absorbing atoms.

A rough estimate of the power available for absorption in the Hg laser may be developed from the following argument. An intense Hg discharge lamp can be regarded, for frequencies within its emission lines, as a thermal radiation source characterized by some effective temperature T. The laser tube in its elliptical pumping cavity, illuminated by a pump lamp of the same diameter as the laser tube or larger, then appears to be completely enclosed by a thermally radiating surface. Within the linewidth of the pumping transition, this surface is a blackbody emitter at temperature T. The pumping radiation dP per unit area dA within a bandwidth $\Delta\nu$ falling on the outer surface of the laser tube is then given by the blackbody surface emission formula

$$\frac{dP}{dA} = \frac{2\pi\Delta\nu}{\lambda^2} \frac{h\nu}{e^{h\nu/KT} - 1}$$

A reasonable estimate for the effective radiation temperature T in a mercury arc lamp on the 253.7 nm line is something less than but approaching the electron temperature of 12000° K to 15000° K, say 10000° K. For $\lambda = 253.7$ nm, $h\nu/K$ is $\sim 59000^\circ$ K, and the thermal power density at $T = 10000^\circ$ K is $\sim 3 \cdot 10^{-11}$ W/cm^2 Hz^{-1}. For a doppler linewidth $\Delta\nu \cong 1$ GHz this gives ~ 30 mW/cm^2 for the 253.7 nm pump line. The total pumping power into a 70 cm long by 4 mm diameter laser tube is then ~ 3 W. Typical pump lamps used with this laser can in fact deliver ~ 3 W at $\lambda = 253.7$ nm and ~ 0.25 W at the less efficiently generated 404.7 nm line. If we assume 10% of the total Hg atoms are in $^3P_0$, and the total atomic Hg density is 10^{14} cm^{-3}, then $R_0 = 6000$ sec^{-1} and $R_p = 3000$ sec^{-1}.

Using these pump rates the unsaturated round-trip gain in this laser tube as a function of nitrogen pressure is plotted in Fig. 3. At high nitrogen pressures, the gain may fall more rapidly than indicated due to pressure broadening of the 404.7 nm line. However, the actual effect depends strongly on the lineshape of the lamp emission. For this reason, effects of nitrogen pressure on R_p have not been included.

Some typical predicted values of the populations of the mercury levels and some interlevel flow rates are shown in Fig. 4. There are some important features that should be noted. First, the ground state population is significantly depleted, with ~ 17% of the total Hg density in the $^3P_0$ level. It can be seen that a very large fraction of the pumping at 253.7 nm is effective in producing metastable $^3P_0$ Hg atoms. The decay time of $^3P_0$ is ~ 50 μs . The upward pumping rate out of $^3P_0$ is small relative to the decay of $^3P_0$ to $^1S_0$. Hence, the $^3P_0$ population is not expected to be significantly influenced by the 404.7 nm pumping. The relatively small densities in the laser levels are worthy of note. This is reflected in the small gain.

Gain Saturation and Power Output

The variation of the laser power output with nitrogen pressure is most easily derived by returning to the original rate equations for the laser levels, Eqs. (4) and (5). For simplicity, we write:

$$t_4 = (A_4 + K_4)^{-1}$$
$$t_{43} = (A_{43} + K_{43})^{-1}$$
$$t_3 = K_3^{-1}$$
$$t_s = A_{43}^{-1}$$

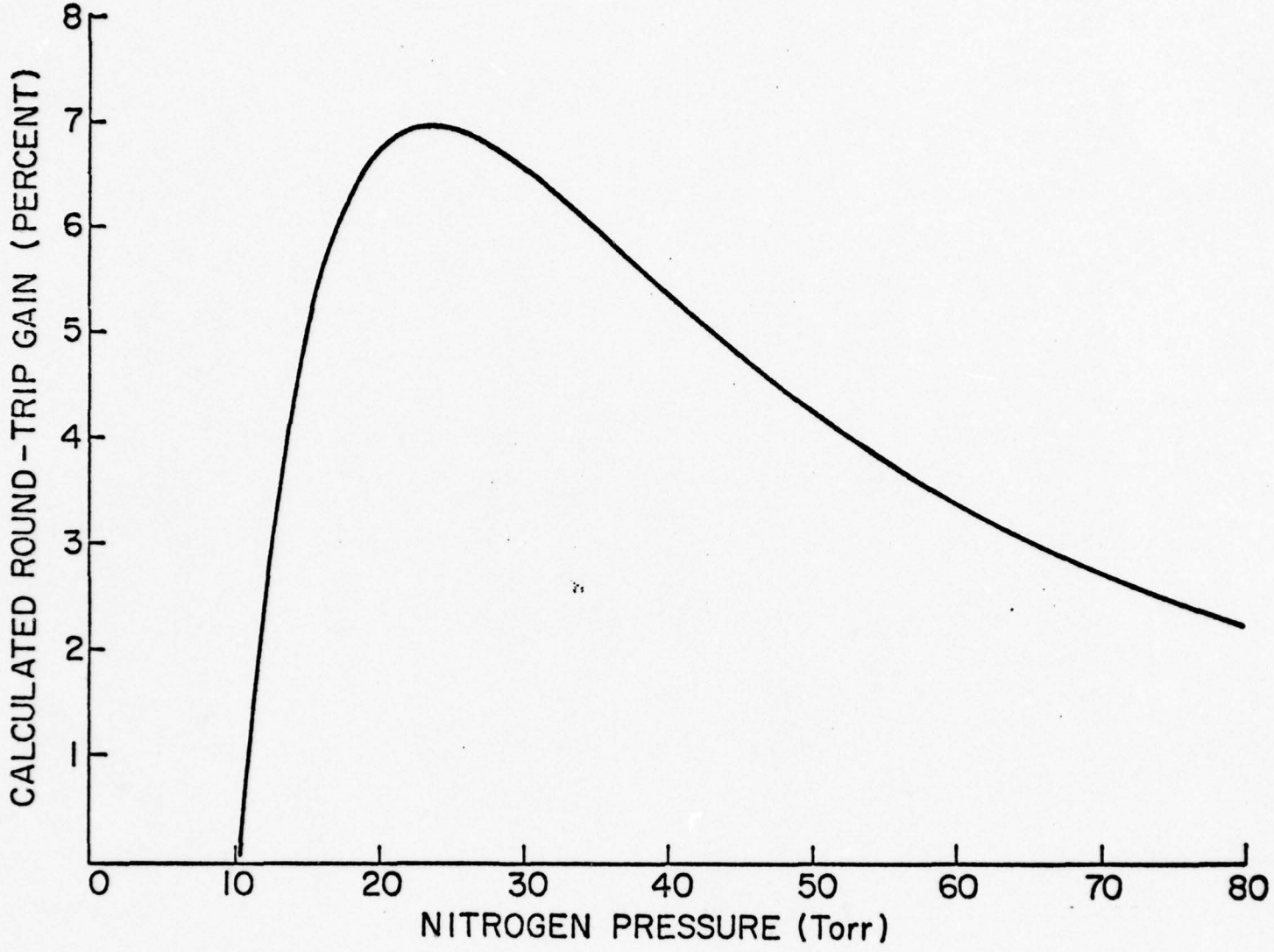

FIG. 3--Calculation of unsaturated round-trip laser gain vs. nitrogen pressure.

TYPICAL POPULATIONS AND FLOW RATES AT 30 Torr

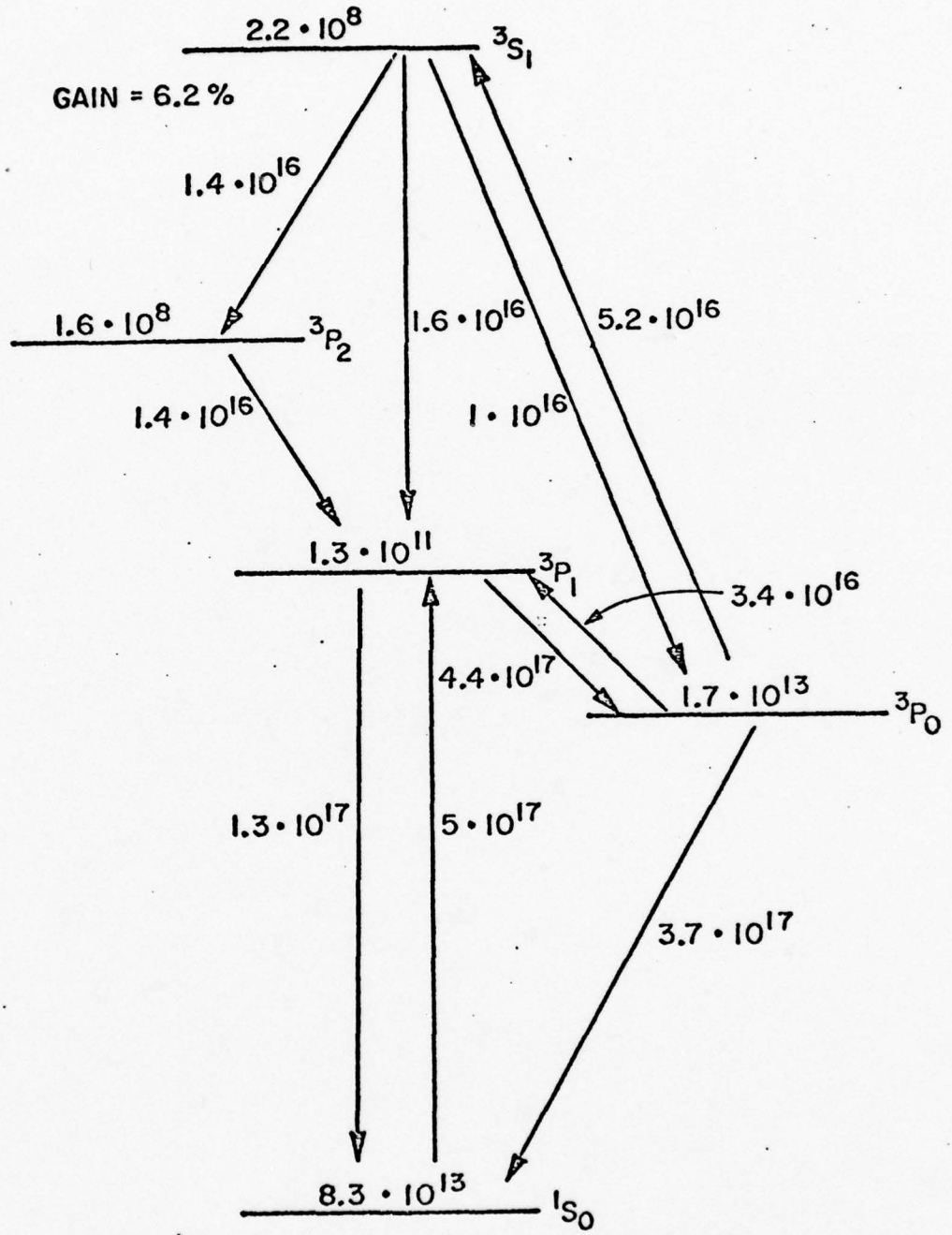

FIG. 4--Rate-equation calculation of Hg level populations and interlevel flow rates.

Then the equations can be rewritten as

$$\dot{N}_4 = R_p N_1 - N_4/t_4 - W_{43}(N_4 - g_4/g_3\, N_3) \tag{17}$$

$$\dot{N}_3 = N_4/t_{43} + W_{43}(N_4 - g_4/g_3\, N_3) - N_3/t_3 \tag{18}$$

In this form the steady-state solution is easily found, viz.

$$(N_4 - g_4/g_3\, N_3)_{s\text{-}s} = \frac{N_1 R_p (t_4 - t_3\, g_4\eta/g_3)}{1 + \varphi t_s\, W_{43}} \tag{19}$$

where

$$\varphi = \frac{t_4}{t_s}\,[1 + g_4 t_3(1-\eta)/g_3 t_4] \tag{20}$$

and

$$\eta = t_4/t_{43}$$

The parameter η is a branching ratio for the upper level decay. φ is usually $\approx t_4/t_s$ and is a measure of how much pumping power can be extracted as useful power on the laser transition. In the mercury laser φ is pressure dependent, varying from 0.6 to 0.2 as the nitrogen pressure increases from 20 to 70 Torr. Its decreasing value reflects the fact that the upper level is more rapidly quenched at higher nitrogen pressures.

We may denote the unsaturated inversion density as

$$\Delta N_0 = N_1 R_p (t_4 - t_3 g_4 \eta / g_3) \quad .$$

The laser transition is assumed to be doppler broadened with doppler width $\Delta\nu_D$(FWHM) and to be composed of homogeneously broadened "spectral-packets" of width $\Delta\nu_H$. Then it is easy to show[10] that the exponential gain constant γ at line center (ν_0) , including saturation, is given by

$$\gamma(\nu_0, I) = \frac{\Delta N_0 \lambda^2 \sqrt{\ell n\, 2}}{8\pi^{5/2} t_s} \frac{\Delta\nu_H}{\Delta\nu_D} \int_{-\infty}^{\infty} \frac{\exp[-4\,\ell n\, 2\,(\nu - \nu_0)^2/\Delta\nu_D 2]\, d\nu}{(\nu - \nu_0)^2 + \left(\frac{\Delta\nu_H}{2}\right)^2 + \frac{\varphi\lambda^3 \Delta\nu_H I}{16\pi^2 hc}} \qquad (21)$$

where I is the internal cavity intensity. This expression is easily integrated to yield

$$\gamma(\nu_0, I) = \frac{A\pi}{x} \exp(\alpha_0^2 x^2) \operatorname{erfc}(\alpha_0 x) \qquad (22)$$

in which we define

$$x^2 = \left(\frac{\Delta\nu_H}{2}\right)^2 + \frac{\varphi\lambda^3 \Delta\nu_H I}{16\pi^2 hc}$$

$$\alpha_0 = \frac{2\sqrt{\ell n\, 2}}{\Delta\nu_D}$$

$$A = \frac{\Delta N_0 \lambda^2 \sqrt{\ell n\, 2}}{8\pi^{5/2} t_s} \frac{\Delta\nu_H}{\Delta\nu_D}$$

Furthermore let

$$\beta = \sqrt{\ln 2}\ \frac{\Delta\nu_H}{\Delta\nu_D}$$

and

$$y = \frac{\varphi\lambda^3}{4\pi^2 hc\,\Delta\nu} I = I/I_{sat}$$

which is the usual definition of the saturation intensity. Then the saturated gain $\gamma(\nu_0, I)$ can be expressed in terms of the unsaturated gain $g_0 \equiv \gamma(\nu_0, I=0)$ as

$$\gamma(\nu_0, I) = \frac{g_0}{(1+y)^{\frac{1}{2}}} \exp(\beta^2 y) \frac{\operatorname{erfc}[\beta(1+y)^{\frac{1}{2}}]}{\operatorname{erfc}(\beta)} \qquad (23)$$

If the unsaturated gain [Eq. (14), for example], the cavity losses, output coupling and mode area are known, then this expression can be solved numerically for the laser output power. Alternatively, if the unsaturated gain, the cavity losses, the output coupling, and laser output power are known or measured as functions of nitrogen pressure, then Eq. (23) can be used to evaluate the pressure broadening of the green laser line. This approach will be used in Chapter II.

C. OPTICAL PUMPING — THE EFFECTS OF MERCURY DENSITY AND PUMPING RATES

A general treatment of the problems of optical excitation in mercury-nitrogen mixtures rapidly becomes very difficult, and is beyond the scope

of this work. A complete theory would require a detailed knowledge of the spectral characteristics of the pump lamps on both the 253.7 nm and 404.7 nm pump lines. Real pumping lamps will suffer from various mechanisms which produce broadening and shift of the pump lines, and their lineshapes may be made very complicated by self-reversal and hyperfine structure. In the laser medium, the situation is much the same as regards pressure broadening and shift. In addition, the effects of radiation trapping, diffusion of Hg atoms, and possible depletion of the ground Hg level under intense pumping must be included, since the laser can operate over a rather wide range of mercury densities, pump rates, and bore diameters. All these complications make an analytic theory very difficult. Hence, we will treat these effects separately and in a qualitative way, and attempt to explain their significance in operation of the mercury laser.

Depletion of the Ground State of Hg for Intense Pumping

As a first step, consider a plane wave incident on a slab containing a mercury-nitrogen mixture typical of that used in the laser tube, i.e. 10^{14} cm^{-3} Hg density and 35 Torr N_2 pressure. The variation of the pumping intensity at 253.7 nm , I , as a function of distance into the slab, x , is given by

$$\frac{dI}{dx} = - \alpha N_0 I \qquad (24)$$

As usual, N_0 is the ground state mercury density and α is the linear absorption coefficient. This expression corresponds to a pumping rate $R_0 = \alpha I$. We neglect for the moment the effects of radiation trapping and diffusion, and some of the less important quenching rates. Setting $R_p = 0$, the rate equations for N_0 , N_1 and N_2 are

$$\dot{N}_0 = - \alpha I N_0 + A_{20} N_2 + K_{10} N_1 \tag{25}$$

$$\dot{N}_1 = K_{21} N_2 - (K_{10} + K_{12}) N_1 \tag{26}$$

$$\dot{N}_2 = \alpha I N_0 - (A_{20} + K_{21}) N_2 + K_{12} N_1 \tag{27}$$

$$N = N_0 + N_1 + N_2 \tag{28}$$

The steady-state solutions for N_0 and N_1 are

$$N_0 = \frac{N}{1 + I/I'} \tag{29}$$

$$N_1 = N_0 \cdot \frac{I}{I'} \tag{30}$$

where we have assumed $N_2 \ll N_1$ and defined a saturation intensity I' by

$$I' = \frac{A_{20}(K_{10} + K_{12}) + K_{21} K_{10}}{\alpha K_{21}} \tag{31}$$

We then substitute Eq. (29) into Eq. (24) and integrate with the boundary condition $I = I_0$ at $x = 0$. The result is

$$\frac{I - I_0}{I'} + \ell n\,(I/I_0) = -\alpha N x \tag{32}$$

Using the values from Table I, and using an effective absorption constant $\alpha = 4.6 \cdot 10^{-13}$ cm^2 (See Appendix A for derivation of effective absorption constants), I' is found to be ~ 100 mW/cm^2 at 30 Torr nitrogen pressure. This is of the same order as I_0 in our experiments, 40 mW/cm^2. Therefore, some degree of pump saturation is expected to occur in the laser tube. Departures from an ideal pumping source, such as broadening and self-reversal, will decrease the value of α and make the ground level more difficult to deplete. However, this will be somewhat compensated by a corresponding decrease in the linear absorption term, $\alpha N x$. The net effect is that, for reasonably intense pumping, the absorption depth for 253.7 nm is not very sensitive to the lineshape of the pump source.

Radiation Trapping

It is also clear that radiation trapping is present in the Hg laser tube. In the work of Holstein,[11] it is shown that the effective radiative decay rate A' for a strongly trapped transition is related to the untrapped rate A by

$$A' = \frac{1.6\,A}{k_0 R[\pi\,\ell n\,(k_0 R)]^{\frac{1}{2}}} \tag{33}$$

where R is the tube radius, $k_0 = \alpha N_0$, and it is assumed that $k_0 R \gg 1$. This expression has been experimentally verified.[21] For the $^1S_0$-$^3P_1$ mercury transition, if $N_0 = 10^{14}$ cm^{-3} in a 4 mm diameter tube, $k_0 R \approx 9$. Hence, strong trapping is expected. In fact, $A' \approx 5.5 \cdot 10^5$ sec^{-1}, about 1/15 of its untrapped value. This will have two main effects. First, it enhances the production of $^3P_0$ atoms, since the $^3P_1$ atoms will have more time to be quenched to $^3P_0$. Second, the saturation intensity I' will be much reduced. For the value of A' just given, the predicted saturation intensity $I' \cong 40$ mW/cm^2, which would imply strong depletion of the ground mercury level. However, these two processes oppose each other to some extent, since ground level depletion will reduce the effects of trapping, while trapping tends to increase saturation and hence ground level depletion. The net effect of trapping and saturable pumping should be to make the rate of formation of $^3P_0$ more nearly uniform within the laser tube. This is, we believe, crucial to the operation of the laser.

Consider the effect if these processes were absent. For a pump lamp and laser tube both filled with the same single Hg isotope and having identical doppler profiles, $\alpha = 4.6 \cdot 10^{-13}$ cm^2. With a mercury density of 10^{14} cm^{-3}, $k_0 = 46$ cm^{-1}. Thus the incident pump light would be mostly absorbed in a thin shell at the wall only ~ 0.2 mm thick. In a $^3P_0$ lifetime, the diffusion length is only ~ 0.2 mm, so that the metastable Hg atoms would be formed very close to the walls, and would stay there. Because of the very short lifetime of the $^3S_1$ level, the diffusion length of $^3S_1$ Hg atoms is negligible. Thus, population inversion and gain would be established primarily in this thin ring right at the walls.

The gain in the interior of the tube, where it is most useful, would be very small. Little of the 404.7 nm pump light would penetrate, and there would be relatively few $^3P_0$ atoms available for absorption.

As noted earlier, the 404.7 nm line is not expected to be effected by saturation effects. To perturb the $^3P_0$ level population by optical pumping, R_p would have to be comparable to K'_{10} . It is difficult to make very intense lamps at this wavelength that do not suffer from self-reversal, and this limits R_p to values on the order of 10^3 sec^{-1}, while K'_{10} is about 10^4 sec^{-1} at the Hg densities used in mercury lasers.

Effects of Mercury Density

In terms of laser operation, the foregoing should make clear the difficulties of making more than qualitative statements. We expect the laser gain to rise with increasing mercury density, until the tube has reached an optimum optical thickness for the combined 253.7 nm and 404.7 nm pumping lines. At higher mercury densities, metastable $^3P_0$ atoms will be formed progressively closer to the walls. This will increase diffusion losses to the walls, and the increasing ground state mercury density will also more rapidly quench the metastable atoms through other mechanisms. However, as the overall Hg density rises, the population of $^3P_0$ Hg atoms is expected to vary rather slowly with increasing Hg density over a moderately broad range. In addition, radiation trapping has been shown[18] to produce a more sharply peaked radial distribution than J_0 , and this effect also increases with increasing mercury density. At some value of

Hg density, the gain at the center of the tube will begin to fall. Smaller diameter tubes will show the same behavior at higher mercury densities. These effects will depend also on the pumping strength and spectral properties of the pump lamps.

D. ISOTOPIC MIXING IN Hg LASERS

The previous sections have implicitly assumed only a single mercury isotope in both laser tube and pump lamp. Since there are significant isotope shifts in the transition frequencies among the seven naturally occuring Hg isotopes, one would expect significant degradation in performance if multiple isotopes were employed. The emission from a multiple isotope lamp is divided among the various isotopic and hyperfine lines, while the upper laser level populations in a multi-isotope laser tube would also be divided among the isotopes, giving a broadened and lowered gain profile.

Experimentally, laser action was first obtained in our laboratory in a system where both pump lamp and laser tube contained a natural isotopic mercury mixture. Direct comparison of these multiple-isotope results with later more detailed experiments using single isotopes was not possible because of the major changes in lamp design between these experiments. Detailed comparisons were made, however, using a single isotope lamp to pump both single and multi-isotope laser tubes. Use of a multi-isotope laser medium was found to decrease the effective gain by ~ 20% as compared to a laser tube filled with a single isotope. This reduction indicates that isotopic mixing effects in the laser medium are of great

importance in determing the sharing of optical excitation and laser gain among multiple isotopes.

The isotope shifts and hyperfine structure of the 253.7 nm, 404.7 nm, and 546.1 nm mercury lines[22] are depicted in Figure 5. To treat a specific example, we shall assume that the laser is filled with mercury of natural isotopic abundances, and is pumped by a lamp containing the single mercury isotope Hg^{202} as in our experiments. If the lamp radiation at 253.7 nm is not broadened appreciably beyond the expected doppler width shown in Fig. 5(a), then the pumping on 253.7 nm is expected to be quite isotope specific, i.e. only Hg^{202} atoms are pumped to $^3P_1$ and form Hg^{202} ($^3P_0$) by nitrogen quenching. However, Vienne-Casalta and Barrat[20] have shown that if the metastable $^3P_0$ lifetime is sufficiently long, a high probability exists that Hg-Hg collisions will spread the excitation of $^3P_0$ atoms among the several Hg isotopes. In their view, collisions of the form Hg^{202} ($^3P_0$) + Hg^x ($^1S_0$) $\longleftrightarrow$ Hg^{202} ($^1S_0$) + Hg^x ($^3P_0$) are responsible for this mixing process (x is the atomic mass of some other mercury isotope). Further mixing will occur between all the other unpumped isotopes as well.

In an effort to explain the potential effects of this process, a steady-state rate equation analysis will be used to find an expression for the relative mixing among the isotopes in the $^3P_0$ level. This will be followed by a qualitative discussion of the effects of $^3P_0$ mixing on laser gain.

Let us define the population densities of the optically pumped Hg^{202} isotope as $[^1S_0] = n_0$, $[^3P_0] = n_1$, $[^3P_1] = n_2$. Then we define the

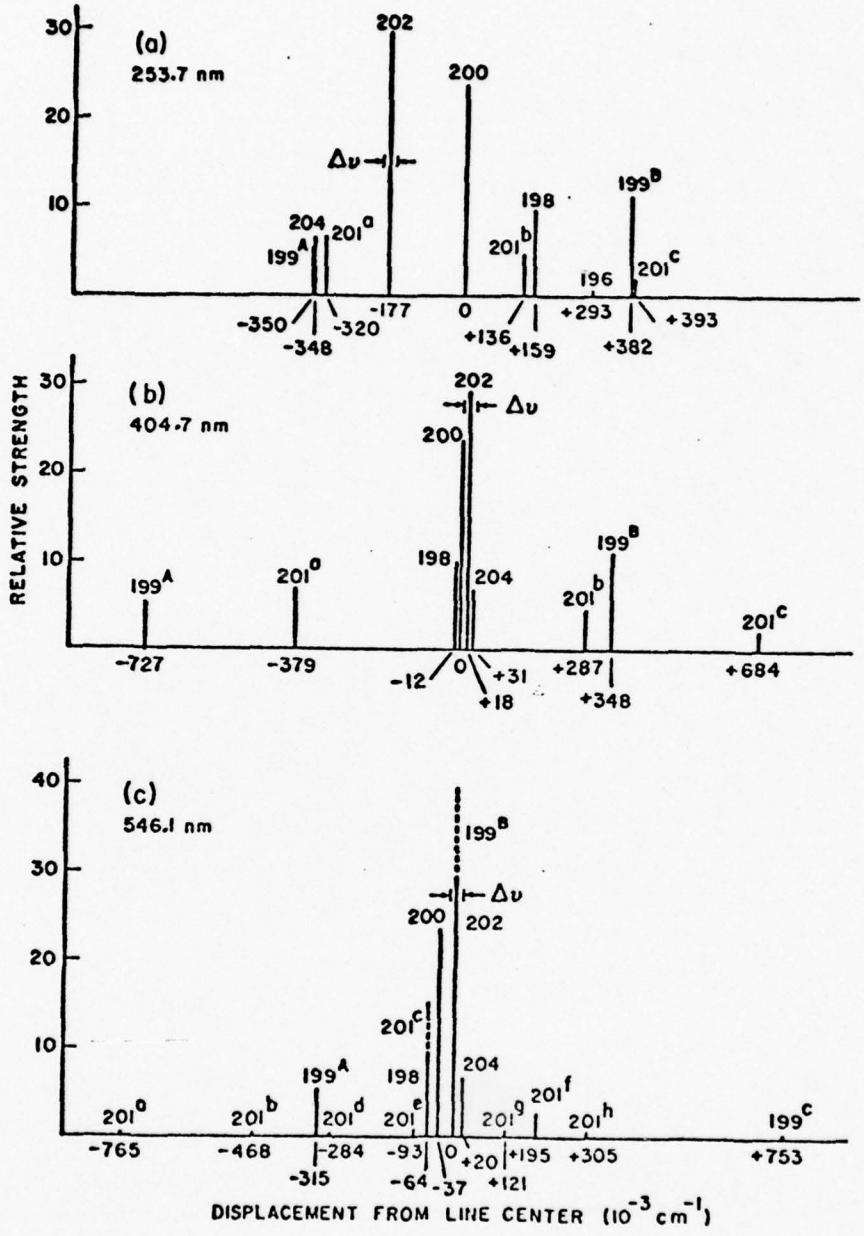

FIG. 5--Hyperfine structure of pumping and laser lines for natural Hg.

population densities of the i-th unpumped mercury isotope as N_{0i}, N_{1i}, N_{2i} by analogy with our previously used notation. Then we can write down rate equations:

$$\dot{n}_0 = -R_0 n_0 + K'_{10} n_1 + \gamma_2 n_2 - \kappa n_0 \sum_i N_{1i} + \kappa n_1 \sum_i N_{0i} \tag{34}$$

$$\dot{n}_1 = K_{21} n_1 - (K_{12} + K'_{10}) n_1 - \kappa n_1 \sum_i n_{0i} + \kappa n_0 \sum_i N_{1i} \tag{35}$$

$$\dot{n}_2 = R_0 n_0 - (\gamma_2 + K_{21}) n_2 + K_{12} n_1 \tag{36}$$

$$\dot{N}_{0i} = K'_{10} N_{1i} + \gamma_2 N_{2i} + \kappa \sum_{j \neq i} (N_{1i} N_{0j} - N_{0i} N_{1j}) + \kappa (n_0 N_{1i} - n_1 N_{0i}) \tag{37}$$

$$\dot{N}_{1i} = K_{21} N_{2i} - (K_{12} + K'_{10}) N_{1i} - \kappa \sum_{j \neq i} (N_{1i} N_{0j} - N_{0i} N_{1j}) - \kappa (n_0 N_{1i} - n_1 N_{0i}) \tag{38}$$

$$\dot{N}_{2i} = K_{12} N_{1i} - (K_{21} + \gamma_2) N_{2i} \tag{39}$$

where we have assumed that all the isotopes have the same radiative decay rate out of $^3P_1$ given by γ_2. The rate constant κ characterizes the mixing process. To simplify the solution, we will assume that the pumping rate R_0 is weak enough that depletion of the ground level for all isotopes is negligible. Thus $N_{0i} \approx N_i$, where N_i is the density of the i-th unpumped isotope, and $n_0 \approx n$, the total density of Hg^{202} atoms. Then the solutions in the steady state are straightforward, and we find

$$\frac{N_{1i}}{n_1} = \frac{\kappa N_i}{\kappa n + K'_{10} + K_{12}(1 + K_{21}/\gamma_2)^{-1}} \tag{40}$$

is an expression for the relative density of $^3P_0$ atoms of the i-th unpumped isotope to the pumped Hg^{202} $^3P_0$ density. We can write

$$\frac{N_1}{n_1} = \frac{\kappa N}{\kappa n + K'_{10} + K_{12}(1+K_{21}/\gamma_2)^{-1}} \tag{41}$$

where

$$N_1 = \sum_i N_{1i}$$

and

$$N = \sum_i N_i$$

The fraction of $^3P_0$ atoms in the i-th unpumped isotope is just $N_{1i}/(n_1 + N_1)$ or

$$\frac{N_{1i}}{n_1 + N_1} = \frac{\kappa N_i}{\kappa(N+n) + K'_{10} + K_{12}(1+K_{21}/\gamma_2)^{-1}} \tag{42}$$

As a typical case, consider an Hg laser filled with natural Hg such that $n \approx 10^{14}$ cm^{-3}, and $N = 2.3 \cdot 10^{14}$ cm^{-3}. The rate constant κ reported by Vienne-Calasta and Barrat[20] is $1.6 \cdot 10^{-10}$ cm^{-3}-sec^{-1}. The total decay rate out of $^3P_0$ is $K'_{10} \approx 2 \cdot 10^4$ sec^{-1}. At 30 Torr nitrogen pressure $K_{12} = 2 \cdot 10^3$ sec^{-1} and $K_{21} = 3.4 \cdot 10^6$ sec^{-1}.

Assuming that radiation trapping reduces γ_2 to $\sim 10^6$ sec^{-1}, we find that $N_1/n_1 \approx 1$. Thus we see that for this case approximately half the Hg^{202} atoms pumped to $^3P_0$ transfer their excitation to other isotopes during their lifetime in the $^3P_0$ level. Using Eq. (42) the fractional populations of $^3P_0$ in the various isotopes have been calculated for this case and are given in Table II.

TABLE II

Isotope	Fractional $^3P_0$ Population
Hg^{202}	0.5
Hg^{200}	0.17
Hg^{199}	0.11
Hg^{201}	0.10
Hg^{198}	0.07
Hg^{204}	0.05

A feeling for the nitrogen pressure and Hg density dependences of these fractions can be developed from inspection of Eq. (42). If the nitrogen is pure, and its pressure is high enough, both diffusion and quenching loss rates adding to K'_{10} are small. In this case, K'_{10} is primarily determined by the quenching of $^3P_0$ atoms to ground in Hg-Hg collisions. Thus, K'_{10} is proportional to the total Hg density $(N+n)$. If $\kappa(N+n) + K'_{10} \gg K_{12}(1+K_{21}/\gamma_2)^{-1}$ as in the case here, then both the effective $^3P_0$ lifetime and the isotopic mixing time depend primarily,

and in the same way, on the total Hg density. Thus, the calculated $^3P_0$ fractions should be relatively insensitive to changes in either nitrogen pressure or Hg density. However, any impurity in the system could increase the $^3P_0$ loss rate K'_{10} substantially. This would make the mixing effects less pronounced, as well as making those effects more dependent on the Hg density.

If the pumping on 404.7 nm by the Hg^{202} pump lamp pumped only Hg^{202} ($^3P_0$) atoms to $^3S_1$, then by Table II the laser gain should be expected to fall by half, since only half of the $^3P_0$ atoms are Hg^{202}. However, a more realistic picture can be formed by consideration of Fig. 5(b) and Fig. 5(c). For these lines, the linewidths at 30 Torr nitrogen pressure are expected to be substantially increased by pressure broadening to about 1 GHz. This implies that the pumping on 404.7 nm is not very isotope specific, especially if the pump line is broadened. The laser gain formed across the $^3S_1$-$^3P_2$ transition is also expected to be less isotope specific; in particular, Hg^{200} ($^3S_1$) and Hg^{204} ($^3S_1$) atoms may also contribute to the gain within the linewidth of Hg^{202}.

The quantitative effect of this on the laser gain is difficult to predict, since the relative shift of the pump line to the absorption line at 404.7 nm is unknown, as are the lineshape and linewidth of the 404.7 nm emission in real pumping lamps. Furthermore, the uncertainty in the value of κ is ~ 30%, while for K'_{10} it is ~ 50%. If we use the minimum value of κ and the maximum value of K'_{10} consistent with these uncertainties, N_1/n_1 is decreased to 0.6, and the fraction of Hg^{200} ($^3P_0$) atoms, for example, is reduced to 0.13.

Let us assume a relatively broad pump line at 404.7 nm which uniformly excites the even isotopes in $^3P_0$, and also assume that it is completely absorbed by these isotopes (this is the most favorable case if these isotopes are to contribute to laser gain). Then the relative isotopic fractions in $^3S_1$ will be the same as given by Table II. The Hg^{200} atoms in $^3S_1$ will then add about 10% to the gain at the center of the Hg^{202} laser line. In other words, the observed laser gain would be ~ 55% of that expected for a single isotope Hg fill.

A more realistic assumption is that the laser tube is not optically thick at 404.7 nm for the unpumped even Hg isotopes, since their $^3P_0$ densities are much less than that of Hg^{202}. If the concentration of Hg^{202} ($^3P_0$) atoms is such that $k_0R = 2$ for the 404.7 nm pump line, then the Hg^{200} ($^3S_1$) contribution to the laser gain is reduced to ~4%. Thus we expect that most of the excitation mixed into the $^3P_0$ levels of the unpumped isotopes will not allow efficient excitation for these isotopes to $^3S_1$, and the laser gain will still be substantially reduced when using a laser filled with a natural Hg mixture.

As mentioned previously, we observed a gain reduction of only ~20% in our experiments. This reduction was, however, independent of the nitrogen pressure as expected. This implies that the ratio K'_{10}/κ was somewhat larger than that calculated above. It is most likely that an impurity in the laser or the gas stream increased K'_{10} markedly, but the value of κ may also be too high. These experimental results are presented in somewhat more detail in Chapter II.

Summary

We have presented a quantitative analysis describing the expected nitrogen pressure dependence of the unsaturated gain and output power of the optically pumped mercury vapor laser. It is also fully adaptable to describe cw 546.1 nm laser action in mercury lasers containing gases other than, or in addition to nitrogen. A qualitative discussion of some important processes in the optical pumping scheme, and a description of the effects of mercury density was given. Further work on measuring quenching rates will increase the confidence with which this model may be used. The potential effects of mixing of optical excitation in lasers containing mixtures of mercury isotopes were described.

A great deal of work remains to be done to understand the optical pumping processes in dense, saturable, and trapped mercury-nitrogen mixtures. It is hoped that some of the problems raised here will spur further work on this very interesting laser system.

CHAPTER II

EXPERIMENTAL WORK

A. INTRODUCTION

In Chapter I, an analytical model of the optically pumped cw mercury vapor laser at 546.1 nm was presented. This model was developed in an attempt to explain the behavior of the laser as a function of nitrogen pressure, mercury density, pumping rates, and laser tube diameter. Here the results of a series of experiments in which these parameters were varied is presented. It will be seen that the theory is quite successful, especially in regard to nitrogen pressure dependence. The departures that are observed may well be due to spatial effects, which do not easily submit to analysis. These measurements will provide an accurate picture of expected laser performance, and can serve as a guide to the design of practical mercury vapor laser systems.

The main difficulty encountered when working with this laser is its extreme sensitivity to gaseous impurities, such as hydrogen or oxygen. It is our experience that, if the laser is to be operated successfully over an extended period, extremely careful and clean technique is required. This laser is a low gain system, so the optics used must be selected for low scattering losses. In short, the mercury laser is

very dependent on careful experimental work. Before proceeding to the results a detailed description of the apparatus and some useful techniques will be given.

B. APPARATUS

Sealed-off Hg laser tubes have been successfully operated in this laboratory.[1,2] However, for experimental flexibility all the measurements reported here were performed using a slowly flowing gas system. The laser tube and optical pumping apparatus are shown in Fig. 6, and the gas handling system is shown in Fig. 7.

In Figure 6, the laser tube is shown placed at the common focus of a polished aluminum optical pumping cavity, in the form of double ellipses. The tube, which is of all quartz construction, has an inner tube containing the flowing laser medium surrounded by a coaxial water jacket of 2.2 cm o.d. The laser tubes used in the experiments were all 80 cm long, 70 cm of which was within the pump cavity. Brewster angle windows were installed on the tube ends with greaseless O-ring tapered joints. These joints allowed full rotation and some translation of the windows, so that reflection and scattering losses could be minimized. Nitrogen gas was admitted to the tube at one end, after passing over a drop of liquid Hg in the U-bend, which was placed in a temperature-controlled water bath. The nitrogen-mercury mixture then flowed slowly through the laser tube and back to the gas handling system. Mercury arc pumping lamps were installed at either or both outside foci of the ellipses. The lamps were mounted on mechanical stages to allow positioning them for best focus into

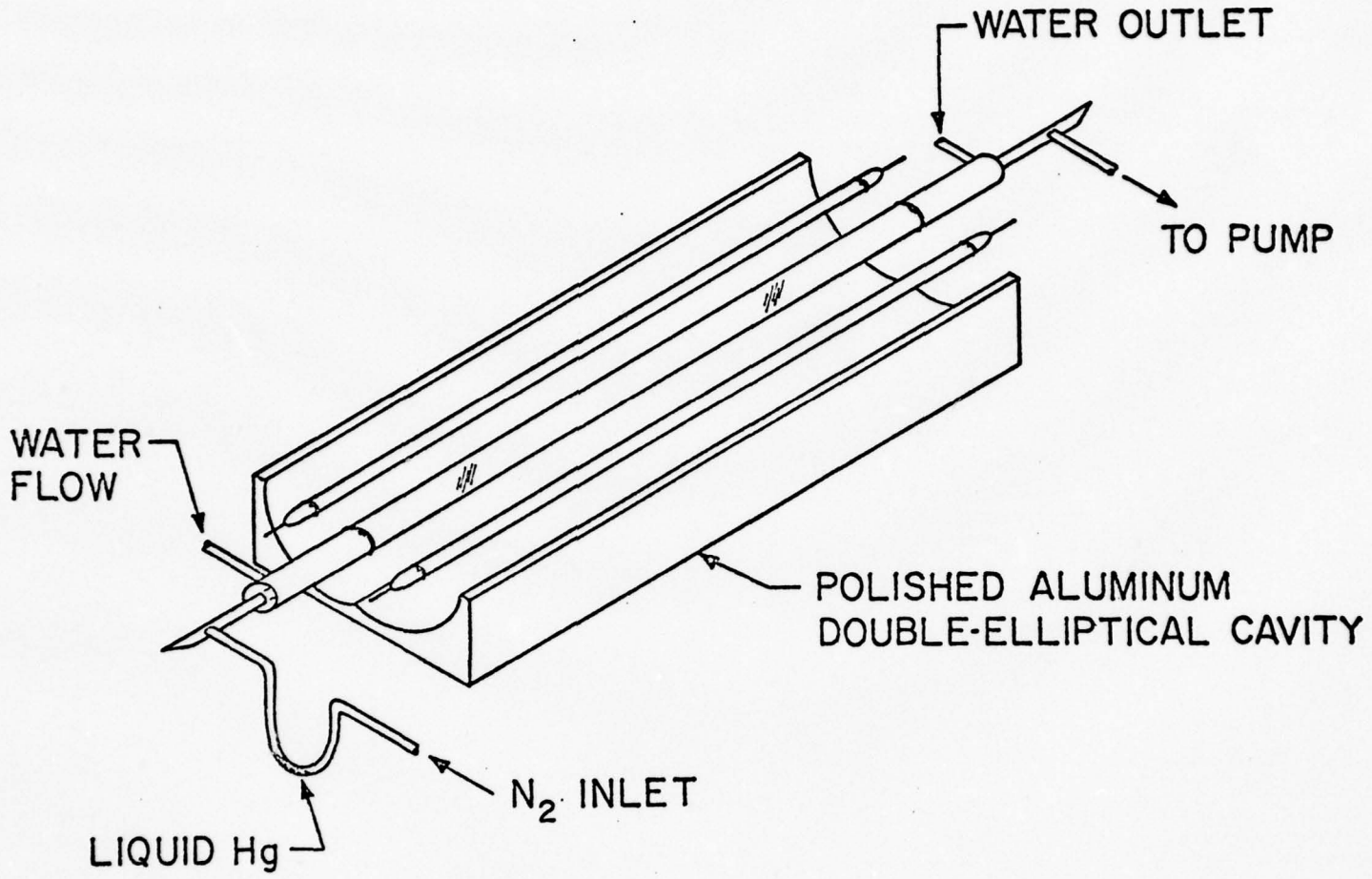

SCHEMATIC OF $Hg-N_2$ LASER EXPERIMENT

FIG. 6--Mercury laser and optical pumping apparatus.

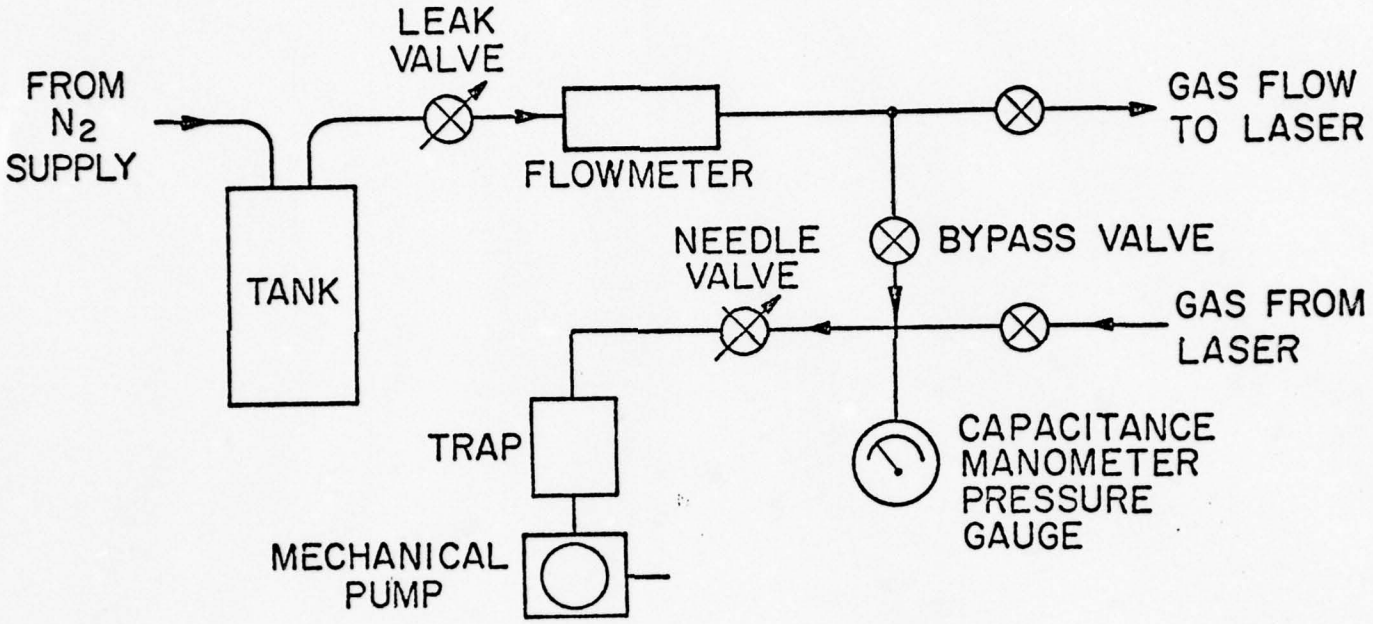

FIG. 7--Mercury laser gas flow system.

the laser tube. Both the lamps and the laser tube were temperature stabilized along their length with flowing deionized water at 47° C.

Besides experimental convenience, a flowing system is somewhat forgiving from the standpoint of cleanliness. In the laser, the intense ultraviolet radiation from the pump lamps tends to drive gases from the laser tube walls and break down grease molecules. In a sealed-off laser tube, these adsorbed gases and impurities can be driven off during processing by prolonged high temperature vacuum bakeout. In the flow system, they are continually swept from the laser, so that harmful concentrations do not build up. Of course, the flow system is not a panacea. An impurity that is present in more than trace amounts and is not very volatile will not be cleaned up by flow in any reasonable time. This is most serious if the impurity is in the laser tube or located anywhere in the incoming gas stream. Thus, all such sources of contamination must be removed prior to operation with careful and thorough cleaning of all parts of the laser and flow system. Also, great care must be taken to avoid virtual leaks in any component. Thoroughness in cleaning and care in construction are of paramount importance. It is impossible to stress this too strongly. With proper cleaning, the flow system will purge itself of water, oxygen, and other atmospheric contaminants with just a few hours of flowing gas through it. Of course, this is academic if the gas used to operate the laser is not pure. We have found that oxygen impurities in the nitrogen in concentrations as low as 1 in 10^4 will completely quench the green fluorescence. In our experiments, Matheson research-grade nitrogen was used exclusively, and gave no problems.

In the gas handling system, Fig. 7, nitrogen gas from a tank or bottle is first stored in a gas tank of ~ 5 l volume at or above atmospheric pressure. The use of such a tank eliminates the potential problems of gas pressure regulators, which are hard to service and generally of questionable cleanliness. The gas is metered into the laser through a Granville-Phillips Model 203 leak valve in series with a modified rotameter-type flowmeter. After passing through the laser tube the gas pressure was measured at the output from the laser tube using a capacitance manometer. The used gas then passed through a small-orifice needle valve, a molecular sieve trap, and into a mechanical pump. Additional valves were installed to allow the laser tube to be changed while gas could continuously flow through the system. Simultaneous adjustment of the leak valve and needle valve set the flow rate and the pressure. The flow rate should be low to ensure complete saturation of the nitrogen as it passed over the mercury drop. In our experiments, the flow rate was ~ 1 scc/min, corresponding to a complete change of the gas every 30 seconds.

In our experiments, the water bath containing the mercury filled U-tube was operated well above room ambient temperature for long periods. To avoid mercury condensation and the consequent loss of Hg vapor pressure control, all the components between the mercury drop and the water jacket of the laser were heated with tape to ~ 60°-70° C.

The single-isotope mercury used in most of our experiments was purchased in the form of HgO powder. It had an isotope enrichment to > 95% Hg^{202}. To prepare it for use in the laser, it was first dissolved in a dilute solution of nitric acid and deionized water. Then the mercury

was removed from solution by electro-plating it onto a thin gold strip. This strip was then inserted about half-way down into the input side of the U-tube. The laser was pumped out to ~ 5 μ nitrogen pressure and the bottom section of the U-tube was chilled. Gentle heating of the plated foil strip drove the Hg from the strip and into the chilled section. Then the strip was removed and the laser pumped out. The laser tube was then purged with rapidly flowing nitrogen for several hours before operating the laser.

Pump Lamps

Early in this work, the laser was operated successfully using commercially available mercury germicidal lamps excited at 60 Hz.[1] These lamps were far from optimal for pumping, because they could deliver little useful power to the laser tube. This was due to: (1) They could not be operated well at high discharge currents; (2) Their diameter was too large for efficient imaging into the laser volume; (3) They could not be conveniently temperature stabilized; (4) They were filled with mercury of natural isotopic composition, which is not as efficient as a lamp filled with a single isotope.

The requirements for a good pump lamp can be inferred from the above. An efficient lamp will operate at relatively high discharge currents to provide high pumping intensities. For this power to be useful, the lamp must be the same diameter as the laser tube, ~ 4 mm. It must operate using only a single mercury isotope and be easily temperature stabilized. Several lamp designs have been used. They have all featured a water

cooling jacket along their length, both to provide temperature stability and to keep the mercury density in the lamp at a low value, so that the 253.7 nm line is not strongly self-reversed. The use of single mercury isotopes adds another constraint. These enriched isotopes are very expensive, so only a very small quantity can be used. This rules out the use of mercury-pool type electrodes. The cataphoretic transport of mercury to the cathode region is quite rapid in lamps operated at the current densities required for laser pump lamps, on the order of 2-3 mg/hour of operation. Thus, the small supply of mercury in a typical lamp, ~ 15 mg, would be completely transported to the anode in 5-6 hours of operation.

A lamp designed by Artusy[2] in this laboratory has been quite successful in solving these problems. The interested reader is referred to the Reference 2 for a detailed description of the design and processing of this lamp, but a brief description is appropriate. This high-intensity dc-excited mercury arc lamp has the form of a long rectangular ring. One side contains the arc bore, 4 mm i.d., surrounded by a coaxial water jacket of 2.5 cm o.d. The opposite leg, 4 cm dia, forms a diffusion-driven return path for the mercury, which is pumped by cataphoresis to the cathode, to return to the anode end. This leg also contains corrugated metal baffles to suppress the discharge in the mercury return path. These two sides of the lamp were ~ 1 m long and ~ 10 cm apart, connected to each other at each end with 2.5 cm o.d. tubing. A directly-heated tungsten-matrix dispenser cathode (manufactured by Spectra-Mat, Watsonville, California) was used. These lamps must be transparent to pump radiation at 253.7 nm, and accordingly were fabricated entirely of fused silica tubing.

The lamp used in this work was filled with ~ 15 mg of Hg^{202} and 300 mTorr of argon. In operation, it is excited by a current regulated dc supply in series with a 100 Ω ballast resistor. The measurements reported here were carried out, except as noted, as a lamp current of 1.7 A. With the water-jacket cooling temperature at 47° C, the voltage across the lamp was 195 V. This lamp has operated successfully for more than 500 hours with little degradation in performance. The power output on the two pump lines was ~ 10 W at 253.7 nm and ~ 1 W at 404.7 nm. Only one such lamp was built, so all these measurements were performed using this lamp alone.

C. GAIN AND POWER OUTPUT MEASUREMENTS

The unsaturated or small-signal laser gain was measured by using two counter-rotating quartz Brewster plates inserted into the optical resonator. As these windows were rotated away from Brewster's angle, the cavity losses increased until threshold was reached. Measuring the angle of the windows allows calculation of the insertion loss, and hence the gain. The drive mechanism for the windows was designed to minimize backlash and vibration, and had a repeatability in angle better than 3 minutes of arc. For convenience, a digital scale was added to allow direct angular readout. Laser power output was measured with a filtered, calibrated PIN-10 photodiode. Errors in both gain and output power were estimated to be about 5%.

The results of gain measurements for laser tubes of various diameters are shown in Fig. 8. Unsaturated round trip gain is plotted vs.

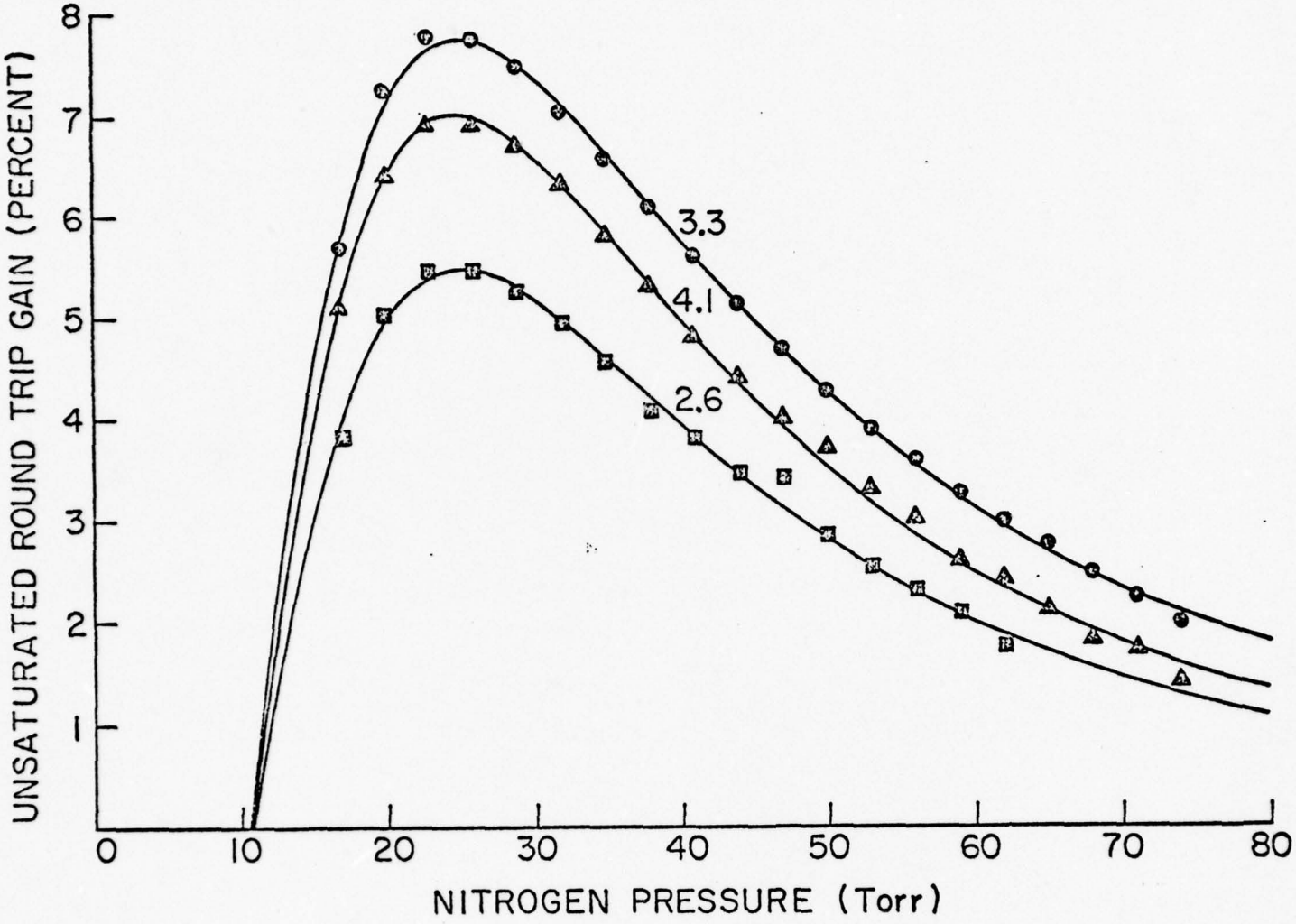

FIG. 8--Unsaturated round-trip gain in Hg laser vs. nitrogen pressure for laser tubes of 2.6 mm, 3.3 mm, 4.1 mm diameters.

nitrogen pressure. The solid curves are calculations based on a least-squares curve fit of these data to expressions of the form

$$g_0 = \frac{\alpha P^2 - \beta P}{\gamma P^4 + \delta P^3 + \epsilon P^2 + \zeta P + 1} L(P) \qquad (43)$$

where g_0 is the unsaturated gain, $\alpha - \zeta$ are adjustable constants, and $L(P)$ is a lineshape function effected by pressure broadening and will be discussed later. This expression was derived in Chapter I as Eq. (16).

It is clear that there is excellent qualitative agreement between theory and experiment. For two reasons, however, it is difficult to go much beyond that. First, the curve-fits are relatively insensitive to changes in some coefficients, especially ϵ and ζ. Also, the coefficients themselves are rather complex combinations of many rate constants. Since the values of some of these rates are not well-known, it is hard to evaluate rates from these data. One very important rate is easily found, however.

First we note that all the curves go to zero at about the same point. The higher the maximum gain, the more steeply these curves cross zero. Thus, the zero of the highest gain case will be less effected by errors in measured gain. In Chapter I, the expression for the unsaturated laser gain was found proportional to $N_4 - g_4/g_3 N_3$. Here N_4 denotes the population density of the $^3S_1$ level, N_3 represents the $^3P_2$ mercury levels, and g_4, g_3 are the degeneracies of these levels. In Chapter I we were able to write N_3 in terms of N_4. In fact,

$$g_0 \propto N_4 \left(1 - \frac{g_4}{g_3} \frac{A_{43} + K_{43}}{K_3}\right) \qquad (44)$$

where A_{43}^{-1} is the spontaneous lifetime of the laser transition, and $A_{43} = 4.5 \cdot 10^7$ sec^{-1} .[3] The quenching rates K_{43} and K_3 are the quenching rates across the laser transition, and out of the lower laser level, respectively. These rates are proportional to nitrogen pressure, so we let $K_3 = t_3 P$, $K_{43} = t_{43} P$, where P is the nitrogen pressure. Burnham and Djeu[4] measured $t_3 = 3.0 \cdot 10^6$ sec^{-1}-Torr^{-1} ± 35%. If P_0 is the pressure at which the gain curve crosses zero,

$$t_{43} = \frac{g_3/g_4 \; t_3 P_0 - A_{43}}{P_0} \tag{45}$$

The 3.3 mm dia. tube exhibited the highest gain, so the values of α and β for that tube were used. $P_0 = \beta/\alpha$, and $\beta = 2.36$, $\alpha = 0.228$. This implies $P_0 = 10.4$ Torr and thus

$$t_{43} = 7 \cdot 10^5 \text{ sec}^{-1}\text{-Torr}^{-1} \pm 50\%$$

which corresponds to a quenching cross section of $0.5 \cdot 10^{-16}$ cm^2. This value is in excellent agreement with the value reported by Burnham and Djeu.[4] This value is extremely sensitive to the values of t_3 and A_{43}, since it essentially involves the difference of two much larger rates. This is why the estimated error is so large.

These data may also be used to estimate the optimum laser tube diameter. To do this we must first take into account the fact that the available pumping radiation for the smaller diameter tubes is reduced, since they are smaller than the lamp. It is a simple matter to show

that the efficiency of elliptical pumping cavities is proportional to the ratio of the diameters of the absorber to the emitter, when the absorbing tube is the smaller. Thus, it is possible to "normalize" the maximum values of the gain for each tube by the inverse of the diameter. This "normalized" gain at ~ 25 Torr for the three tubes used is 6.9, 9.6, 8.7 per cent for the 4.1, 3.3, and 2.6 mm dia. laser tubes, respectively. The smaller tubes are somewhat better, but the estimated experimental errors preclude a choice between the two smaller tubes. To achieve this performance, equivalent lamps with smaller arc bores must be made, but there is no guarantee that they can be made to work as well as the 4 mm dia. lamp used here.

A comparison of experiment with a calculation made in Chapter I is shown in Fig. 9. The solid curve is that curve of the form of Eq. (43) which best fits the data for the 4.1 mm diameter laser tube. The dashed curve is an expression calculated from the values of rate constants found in the literature, using the model developed in the first chapter. Up to about 40 Torr the quantitative agreement is excellent. The more rapid decrease in gain observed at higher pressure may be the result of spatial effects, pressure broadening and shift of the absorption lines, metastable level quenching due to impurities in the nitrogen, etc. Obviously, if more detailed knowledge of the relative importance of these processes were known, the predictive accuracy at high pressures might be enhanced. The very good agreement over the typical operating pressure of the laser, 20 to 40 Torr, gives considerable confidence in the model. It should be pointed out that this model also predicts the behavior of

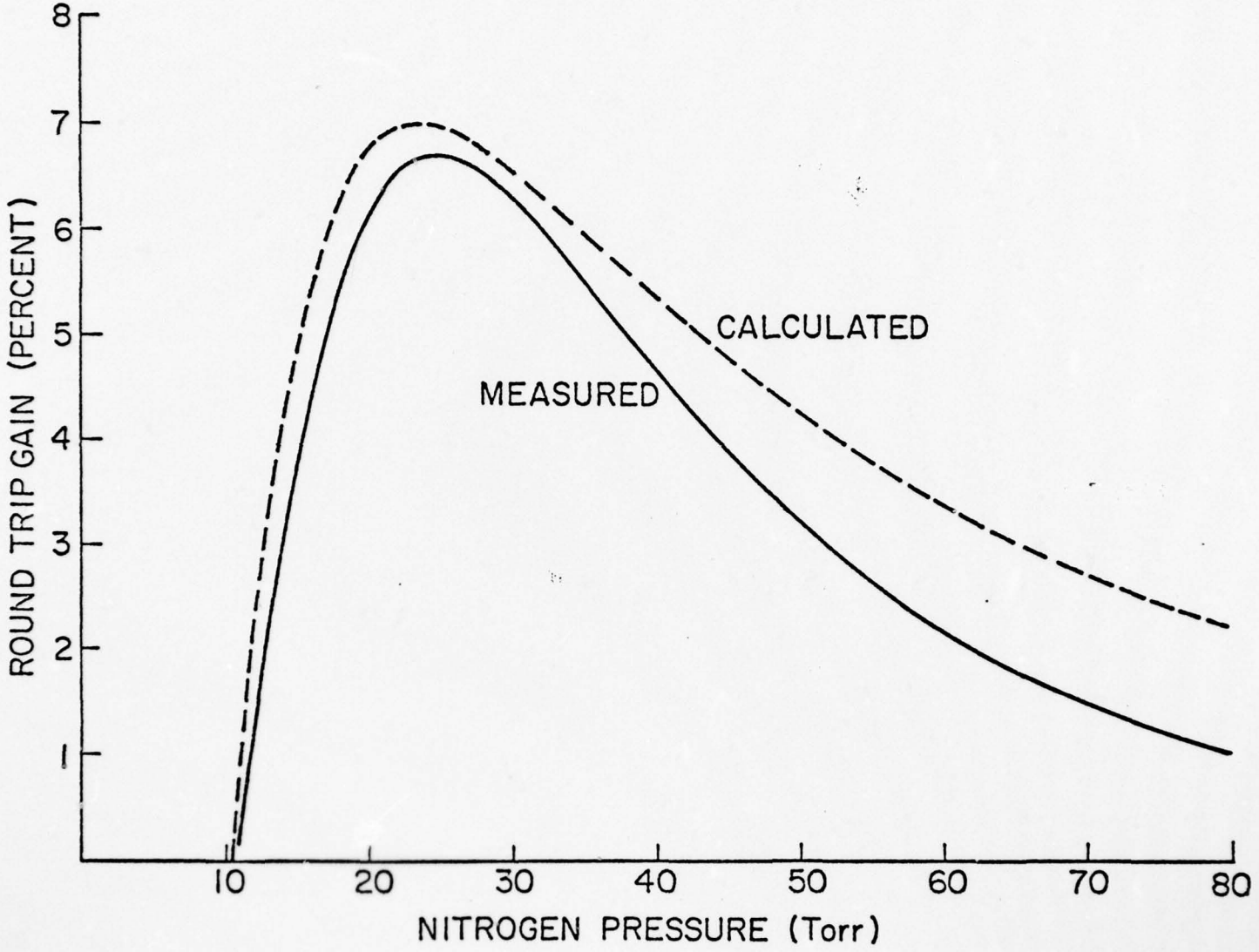

FIG. 9--Comparison of theory and experiment for the Hg laser gain in a 4.1 mm diameter tube.

the absorption of 546.1 nm in the laser tube at pressures below ~10 Torr. Another laser could be used to probe this, and perhaps the values of ϵ and ζ could be found.

A comparison between the pressure dependences of the gain and output power for the 3.3 mm dia. tube, operating multimode, is shown in Fig. 10. Note that the peak power occurs at a higher nitrogen pressure, the power rises more slowly at low pressures, and falls nearly linearly at high pressures. It will be shown that the saturation intensity increases with nitrogen pressure, and this accounts for the behavior observed.

The influence of bore diameter on the available multimode power output is plotted in Fig. 11 for the three laser tubes used. These curves all show the same behavior noted above. Obviously, the maximum efficiency occurs for the largest bore tubes, because it could absorb more pump light, and support very high order transverse modes. A careful look at the figure also shows that the power peaks at different pressures for each tube. This is due to the observed gain variation, and different values of output coupling from the optical resonator. A general rule is that, for a given laser, increasing the gain or decreasing the cavity losses will shift the power peak to higher nitrogen pressures. For a typical laser with optimum output coupling, maximum power output is observed at ~ 35 Torr.

Gain Saturation and Pressure Broadening

It was observed early in our experiments that the laser did not saturate as would be expected for either a pure doppler-broadened or

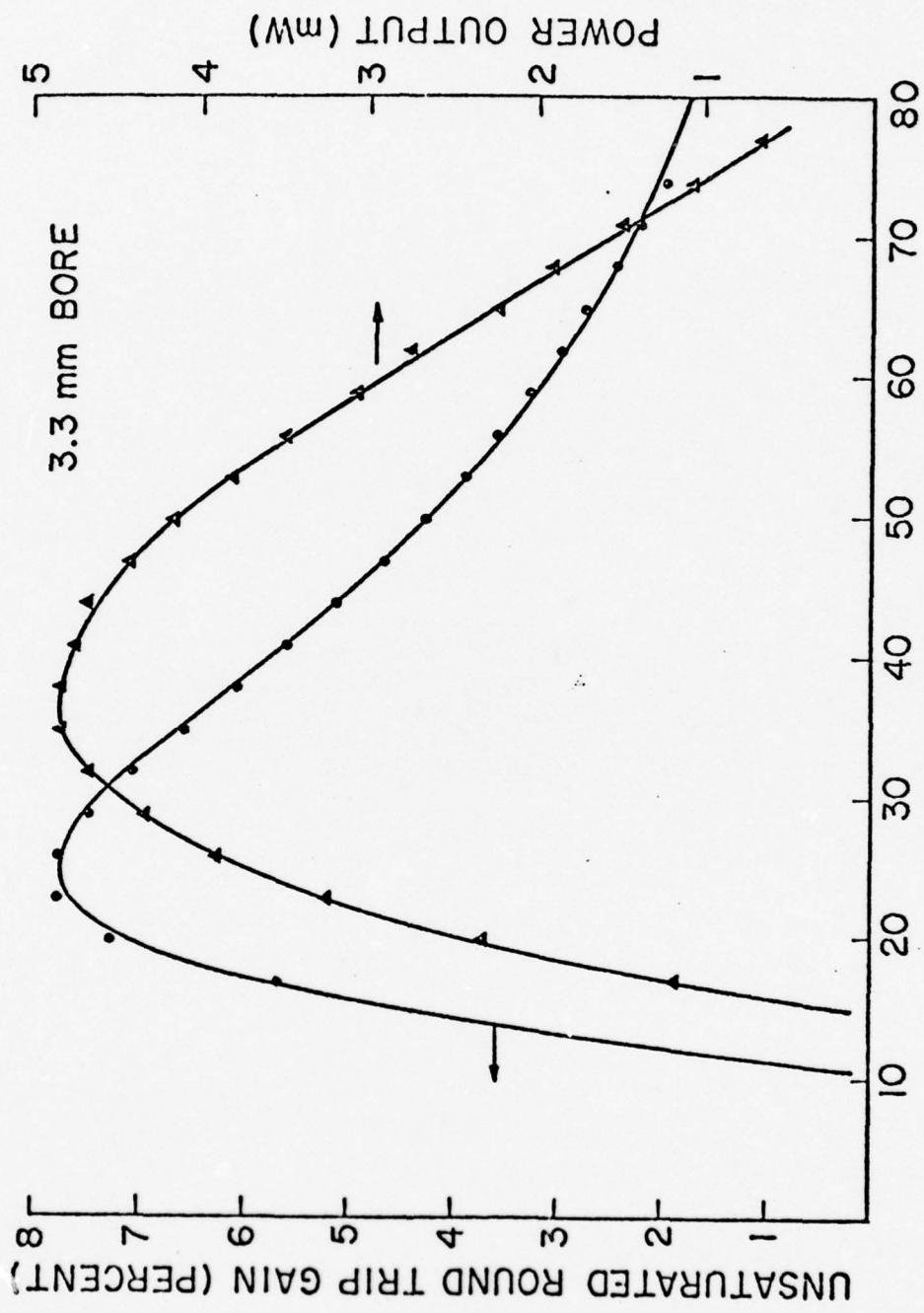

FIG. 10--Comparison of pressure dependence of gain and output power in the mercury laser.

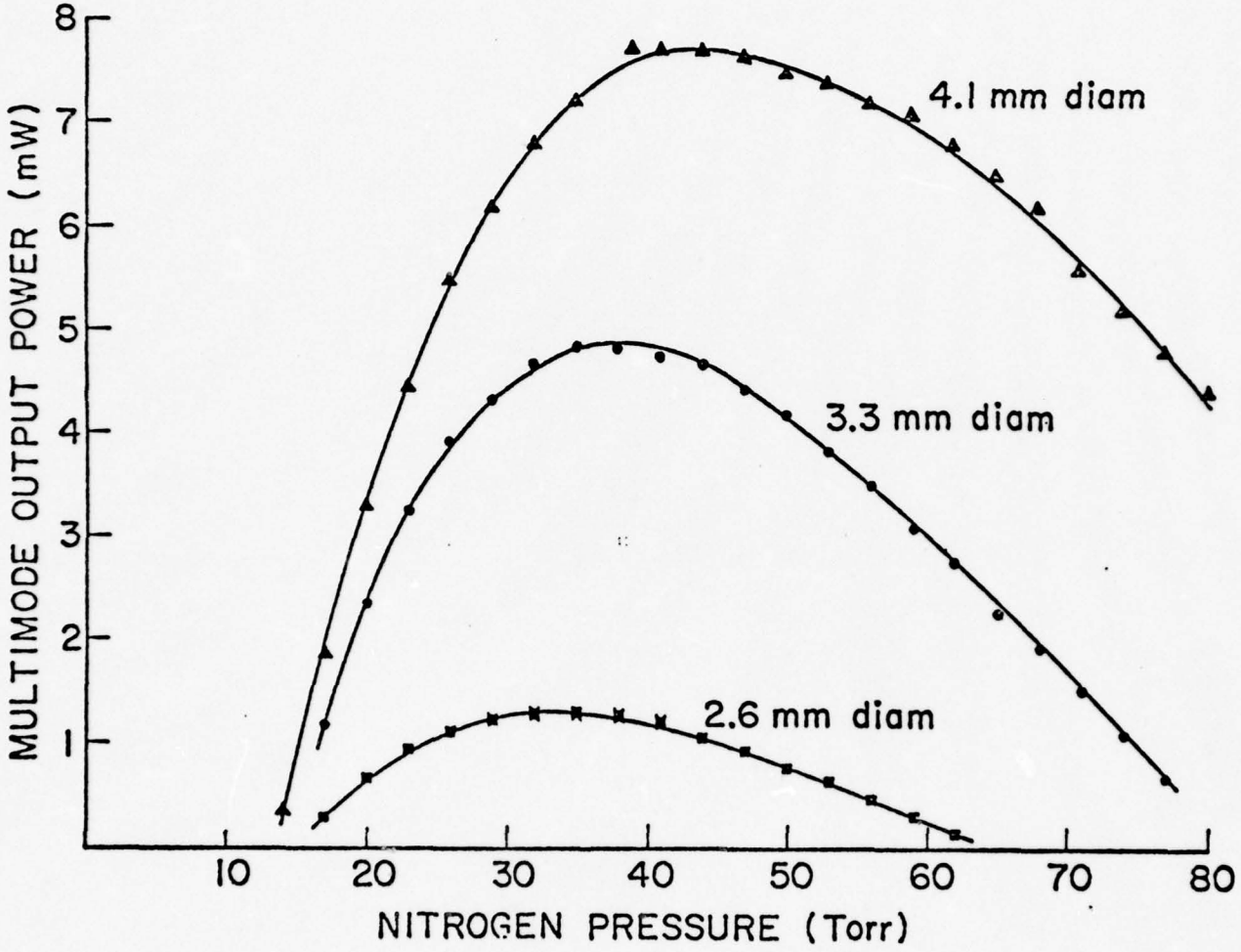

FIG. 11--Multimode output power in Hg lasers of various tube diameters vs. nitrogen pressure.

homogeneously broadened transition. No Lamb dip has been observed. This is most likely due to pressure broadening of the line; cross-relaxation effects may also play a role. We were unable to make a direct measurement of the linewidth, so it is difficult with these data to separate these effects. However, we will show that, under the assumption that cross-relaxation effects are unimportant, excellent agreement with theory is obtained.

An expression for the saturated gain g at the line center, of a laser with a Voigt gain profile was derived in Chapter I (Eq. 23). It is:

$$g = \frac{g_0}{(1+y)^{\frac{1}{2}}} \exp(\beta^2 y) \frac{\operatorname{erfc}[\beta(1+y)^{\frac{1}{2}}]}{\operatorname{erfc}(\beta)} \tag{46}$$

where g_0 is the unsaturated laser gain, and the parameters β and y are:

$$\beta = \sqrt{\ell n\, 2}\, \frac{\Delta\nu_H}{\Delta\nu_D}$$

$$y = \frac{\varphi\lambda^3}{4\pi^2 hc\Delta\nu_H} I$$

The homogeneous linewidth is denoted by $\Delta\nu_H$, the doppler linewidth (FWHM) is $\Delta\nu_D$, and I is the internal cavity intensity. The dimensionless factor φ is a function of nitrogen pressure and is related to the branching ratio of the decay rate across the laser transition to the total decay rate (radiative and non-radiative) of the upper laser level. As the nitrogen pressure is changed from 20 to 70 Torr, φ decreases from 0.6 to 0.2.

Evaluation of the total cavity losses, output coupling, and average mode area in the laser tube allow us to determine all other parameters and to solve Eq. (46) for the only remaining unknown, $\Delta\nu_H$. Using gain and output power data for the 2.6 mm and 4.1 mm diameter lasers operating in the TEM_{00} mode, solutions for $\Delta\nu_H$ were found numerically at several values of nitrogen pressure. The results are shown in Fig. (12). The error bars shown indicate expected random errors. The slope of the line gives a value for the pressure broadening of the 546.1 nm Hg line in nitrogen of 26 MHz/Torr.

The vertical position of the experimental results in Fig. (12) is evidently incorrect, (i.e. shifted downward) since the zero-pressure linewidth should extrapolate to the purely radiative value of ~ 16 MHz, rather than to a negative value as indicated in Fig. (12). However, the behavior of the function on the right in Eq. (46) is such that systematic errors additive in the value of g_0 will cause a shift of the line of $\Delta\nu_H$ vs. pressure, but will not change the slope very much. Since the mercury laser is a low gain system, errors in estimating the cavity losses can lead to relatively large systematic errors (~ 10%). Errors in measuring power output, mode area, and output coupling are multiplicative, since they affect the value of y . These errors will both change the slope and cause a shift, and are therefore more serious. Errors in the factor φ have a similar effect. Use of TEM_{00} mode, carefully calibrated detectors and output mirror coatings have hopefully reduced this problem. We estimate the relative error in the slope as being ~ ± 30% because of all these effects.

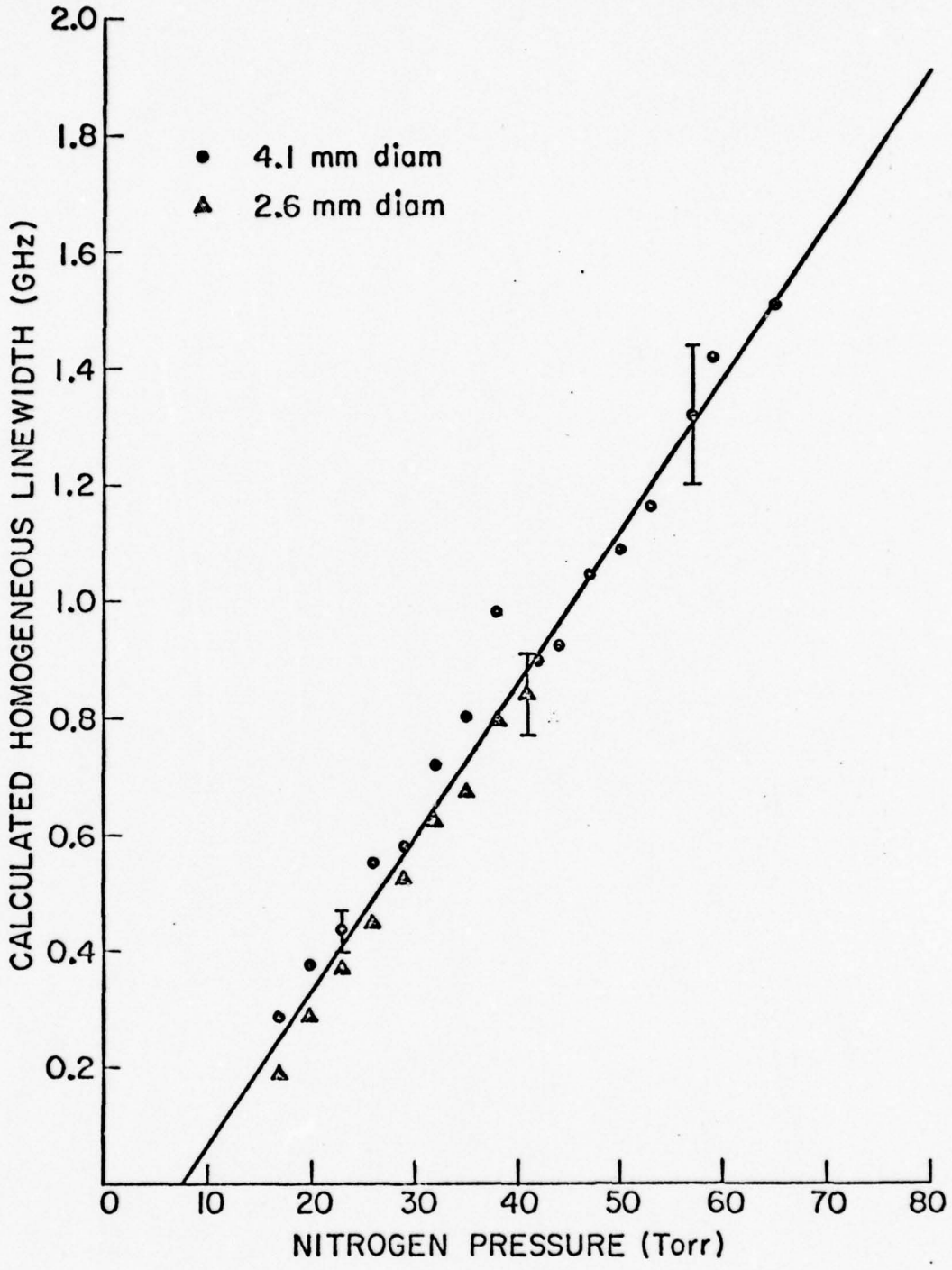

FIG. 12--Calculation of pressure broadening in the Hg laser.

Using this value for the pressure broadening, the saturation intensity $I_{sat} = 4\pi^2 hc\Delta\nu_H/\varphi\lambda^3$ has been calculated as a function of nitrogen pressure as shown in Fig. (13). Its value at 35 Torr, a typical operating pressure is about 12 W/cm^2.

D. PUMPING RATE AND TEMPERATURE EFFECTS

In Chapter I, the relationship of pumping rates and pump lamp spectral characteristics to pump saturation and mercury density effects was discussed. Thus, when results are presented here, it should be understood that they apply specifically to measurements made with the lamp used. Other workers, using lamps with different intensities, or with various amounts of self-reversel, broadening, etc., might see somewhat different behavior than is described in the following.

The rate equation model predicts that the gain should vary linearly with the pump rate at 404.7 nm, since saturation effects for this line should be small. The gain should also increase with pump rate at 253.7 nm, but not in an easily predicted way. When using a single pumping lamp, changes in discharge current produce changes in the intensities of both pumping lines. Thus, the separate dependences could not be obtained with the single pump lamp used in our experiments. However, the total power output of the lamp at 253.7 nm was found to increase by only 10% as the lamp current was varied from 0.8 to 2.0 amperes. The total power output for the 404.7 nm pump line increased by 50% over the same current range. Since these lines were observed through relatively broad spectral filters, only the total output within the line, rather than its line-center value,

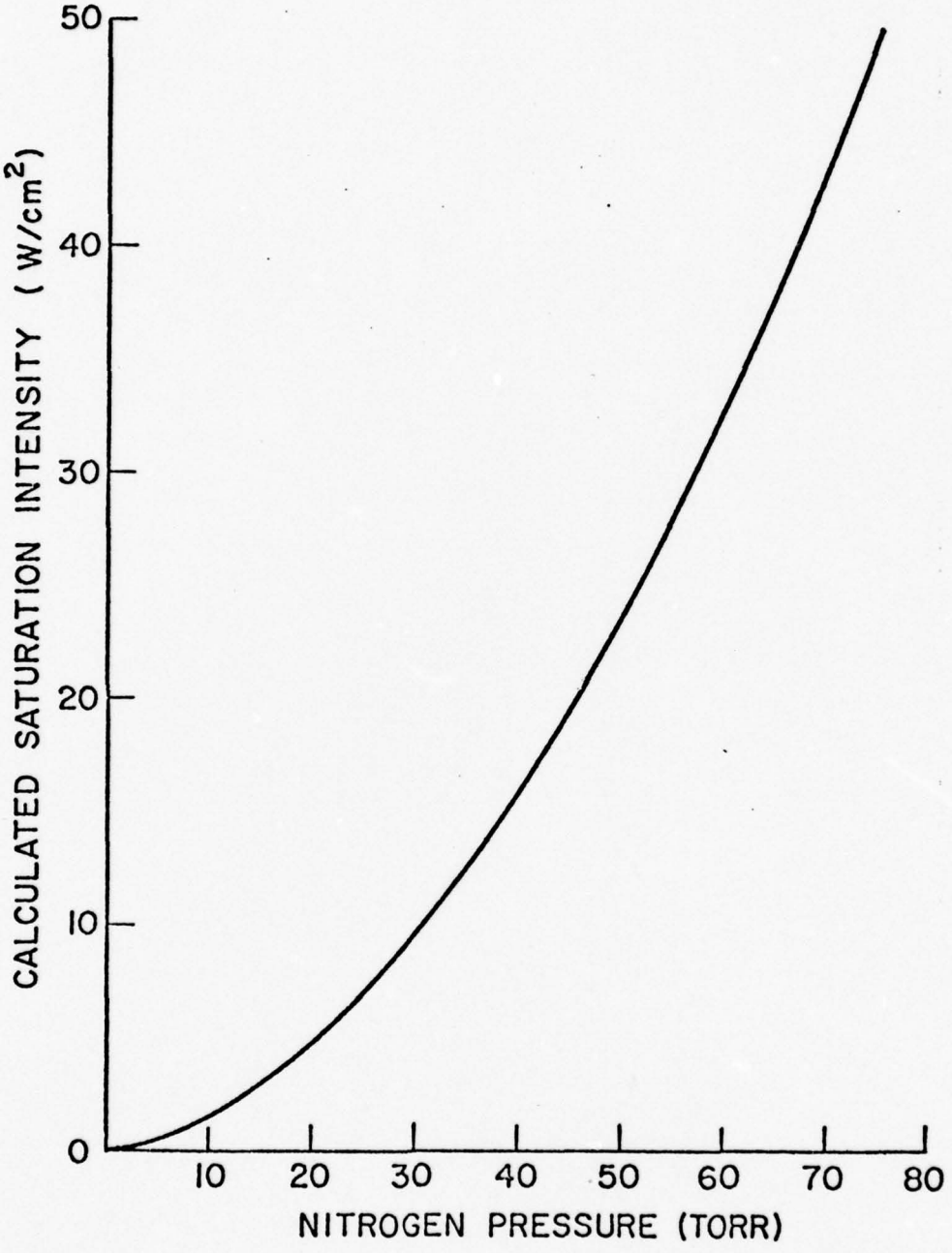

FIG. 13--Calculated saturation intensity vs. nitrogen pressure.

was measured. The unsaturated gain vs. the product of the two line intensities is plotted in Fig. (14). The less than linear increase of the gain with lamp intensity could be due to saturation effects, but it is much more likely that the increased current density in the lamp changed the spectral quality of the pump lines, making them less efficient for optical pumping.

The variation of laser output power with mercury vapor density (shown as the temperature of the water bath surrounding the U-tube) for three different tube diameters is shown in Fig. (15). As expected, the power output (or gain) increases steadily up to a certain point and then reaches a level maximum. Also as expected, smaller bore tubes require higher mercury densities to become maximally opaque to the pumping light. The bath temperature could not be raised above the temperature of the laser water jacket (47° C), so no measurements at higher mercury densities were made. We expected some decrease in power output at high densities, but the decrease, if any, was very small in our experiments. Data for the 3.3 mm dia. tube filled with mercury of natural isotopic composition is included. The power output at 47° C is still rising with temperature. The isotope shift of the 253.7 nm line is much greater than the doppler width, and the 404.7 nm transition is also somewhat resolved with respect to isotope shifts. Thus a single isotope lamp pumps only one isotope. A correspondly higher total mercury density is therefore required for the laser to be optically thick to radiation for only one isotope (natural mercury contains 29% Hg^{202}).

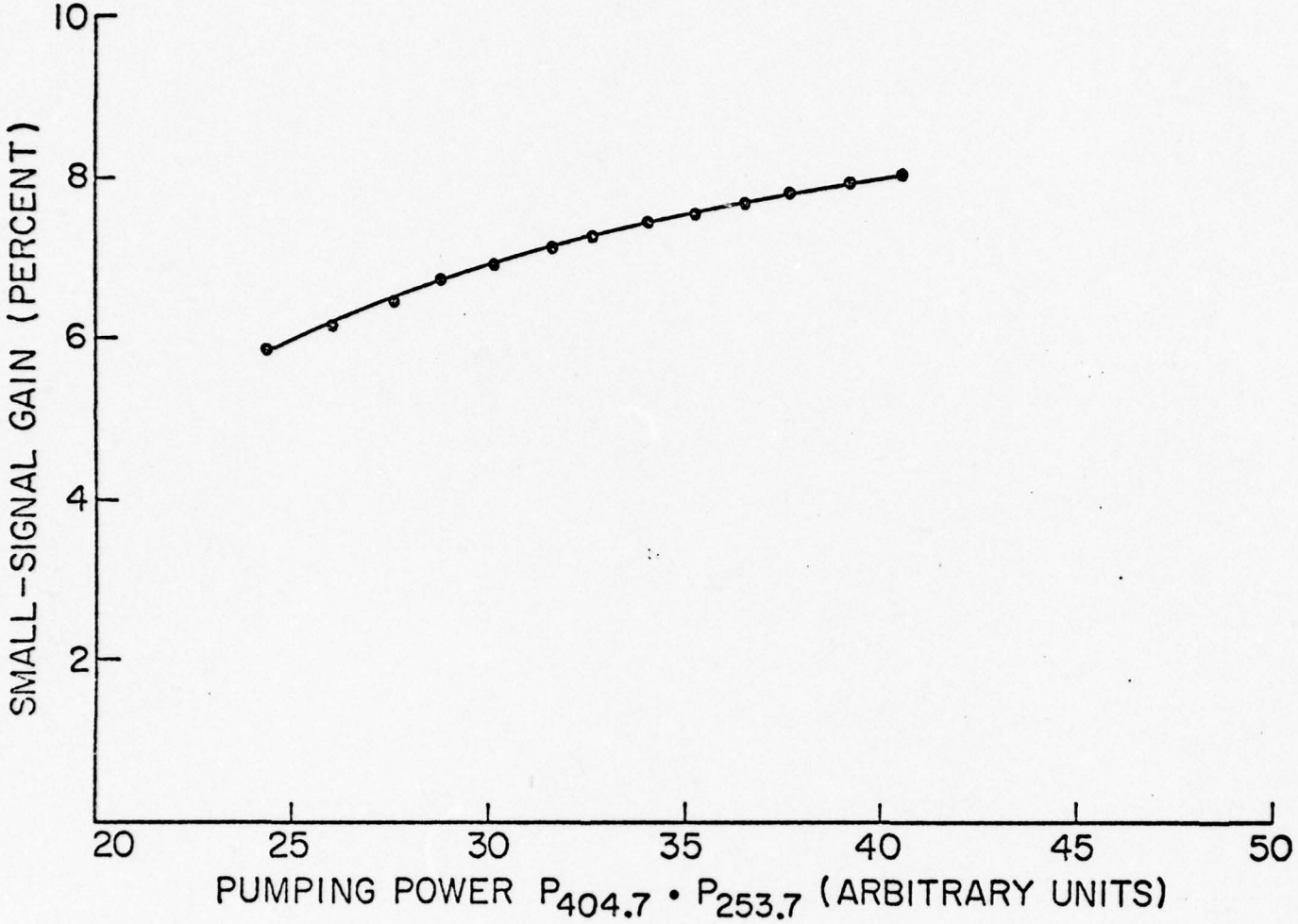

FIG. 14--Variation of gain with pump power. Lamp current varied from 0.8 to 2.0 amperes.

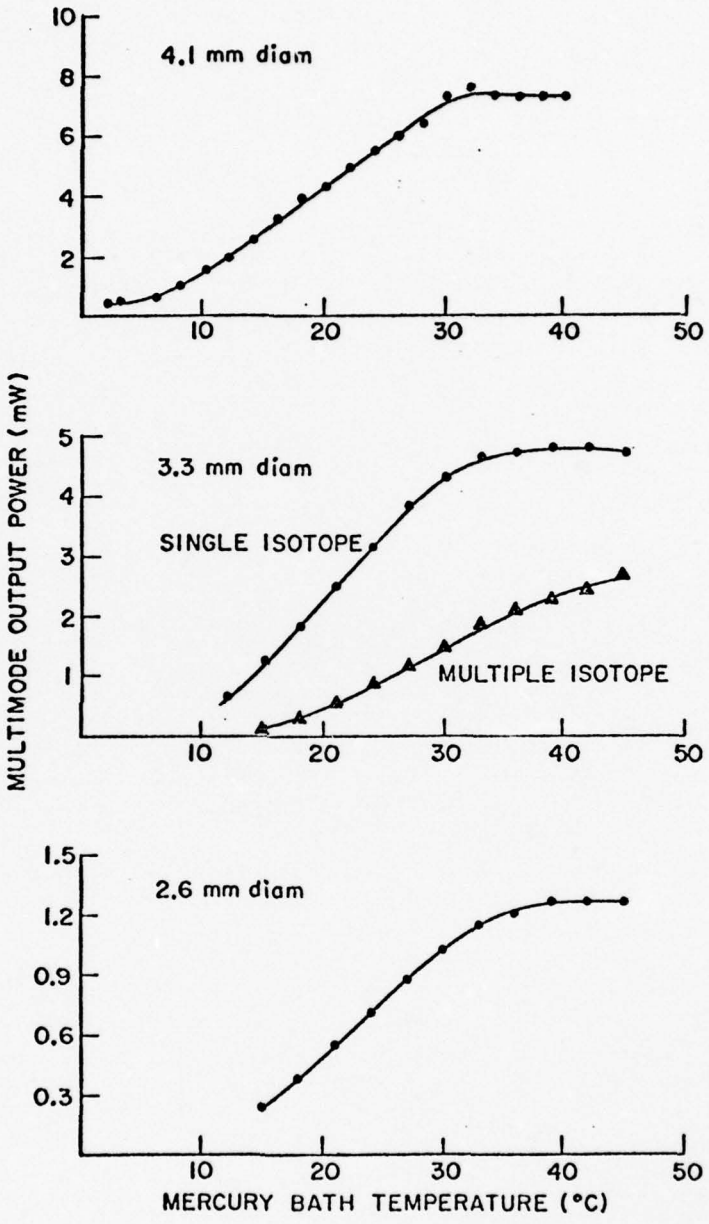

FIG. 15--Effects of mercury density on laser output power.

Since small bore lasers require higher mercury density for most efficient absorption, an additional inference on the effects of bore diameter can be made. The $^3P_0$ level is primarily depopulated by Hg-Hg collisions, according to the work of Callear and Norrish.[6] This implies that smaller bore tubes will have increased $^3P_0$ decay rates. Hence, it will be somewhat more difficult to make them optically thick to the 404.7 nm pump. Also, the small bore tubes will have higher diffusion loss rates (roughly proportional to $1/R^2$). These two reasons may explain the slight reduction in "normalized" gain observed previously between the 3.3 mm dia. and 2.6 mm dia. tubes.

E. MERCURY ISOTOPE EFFECTS

In this section, we will consider the effects of using a mixture of Hg isotopes in the laser tube, pumped by a lamp containing only one mercury isotope (Hg^{202}). The effects are two-fold.

At a given water bath temperature the total Hg density is fixed, and the fractional densities of the individual isotopes are proportional to their isotopic abundances. For the laser to be optimally thick to the pump radiation on both pump lines from the Hg^{202} lamp, the density of Hg^{202} in the mixed-isotope case should be about the same as that found when the laser contains Hg^{202} alone. This means the total Hg density should be about 3.3 times as great. Since the $^3P_0$ decay rate is primarily determined by the total Hg density, we would expect a much increased decay rate for the $^3P_0$ atoms, and with the same pumping power

at 253.7 nm, the population density in $^3P_0$ will be reduced. This will tend to cause a reduction in the laser gain.

Secondly, the effects of isotopic mixing, as discussed in Chapter I, will become important. In Chapter I, we found that under typical conditions of Hg density and nitrogen pressure the laser gain will be reduced when isotope mixing occurs. The excitation into $^3P_0$ is shared to some extent among the various Hg isotopes, but only the population of Hg^{202} ($^3P_0$) is important in forming laser gain. Based on the work of Vienne-Casalta and Barrat,[7] and that of Callear and Norrish,[6] we calculated in Chapter I that the laser gain was expected to fall to about half of its single isotope value when using a natural mixture of Hg isotopes.

In our experiments, the reduction in gain observed between these two cases was much less, only ~ 20%. As predicted by the model developed in Chapter I, this reduction was independent of N_2 pressure. This implies that the metastable decay rate may have been primarily due to some other effect independent of Hg density. In view of the cleaning difficulties and the extreme sensitivity of the $^3P_0$ decay rate to impurities, this is perhaps not so surprising. In addition, the literature values used in calculating the isotopic mixing and decay rates may have large errors, making quantitative predictions inaccurate. Additional work is clearly required to clear up this discrepancy. Direct measurements of $^3P_0$ populations and decay rates, in addition to laser experiments, are probably the best way out of this dilemma.

F. OTHER QUENCHING GASES

Burnham and Djeu[4] have operated this laser using CO as a quenching gas. It has been observed by Wood,[9] among others, that introduction of H_2O vapor increased the intensity of the forbidden line from $^3P_0$, indicating large $^3P_0$ populations.

We achieved laser operation using a flowing mixture of water vapor and mercury, together with argon or helium as a buffer gas to inhibit diffusion losses. Typical output powers of 50 μW were obtained with ~ 7 Torr of helium or argon. The water vapor pressure was unknown, but was certainly < 10 Torr, its vapor pressure at the temperature of the water flask used as a vapor source. Careful measurements could provide a method for determining the rate of collisional de-activation of the $^3P_2$ level by water vapor, since that rate is almost certainly the "bottleneck" in this Hg-H_2O-Ar system.

It has been suggested that using N_2^{15} as a quenching gas merits investigation.[9] Indeed, a simple isotope shift calculation based on the relative masses predicts that its use may improve laser performance by as much as 20%. The decreased vibrational spacing of the N_2^{15} molecule should make the $^3P_1$ to $^3P_0$ quenching rate faster, although this has not been observed.[10] The most important effect expected is to increase the quenching rate of $^3P_2$. With N_2^{14}, the quenching of $^3P_2$ is expected to occur primarily to $^3P_1$. Using N_2^{15}, this rate should be preserved. Indeed, this process may become slightly exothermic. The isotope shift should bring the $v = 0$ to $v = 3$ vibrational transition of the molecule much closer to being resonant with the $^3P_2$-$^3P_0$ energy level spacing.

Assuming equal collision cross-sections for both $^3P_2$-$^3P_1$ and $^3P_2$-$^3P_0$ processes, the effective temperature collision cross-section for the $^3P_2$-$^3P_0$ transfer should about double. This should increase the $^3P_2$ decay rate about 20%, with neglible effects on the repopulation of lower levels. Unfortunately, the N_2^{15} we used in an attempt to test this hypothesis was contaminated with ~ 0.1% oxygen. This amount was sufficient to completely quench the green fluorescence, and, of course, the laser. The use of hot copper traps in the incoming nitrogen stream, used carefully, may allow this test to be made. The use of such traps is non-trivial, though, and time constraints did not allow another attempt.

Summary

The expected operating performance of this mercury laser has been measured under a variety of experimental conditions. With our pump lamps, operated at ~ 340 W dc input, typical gains were measured to be ~ 6% per meter. Output powers of ~ 8 mW were observed in 4 mm diameter tubes operating multimode, although the optimum bore size for gain is about 3 mm. This corresponds to an efficiency of 0.0025%. Improvements in lamp design and gas fill may improve this. A practical gas-flow system for operating the mercury laser has been described. The nitrogen quenching rate across the laser transition was measured to be $7 \cdot 10^5$ sec^{-1}-$Torr^{-1}$. From measurements of gain and output power over a broad range of nitrogen pressures, the pressure broadening of the green laser line was inferred to be 26.4 MHz/Torr. The behavior of

the power output and gain as nitrogen pressure was varied have verified the rate equation model developed in Chapter I. The variations of power and gain with respect to bore diameter, pump rates, and mercury densities were examined, and agree qualitatively with prediction.

Since the overall performance of the laser is determined largely by the quality of the pump sources, their improvement, especially with regard to power output and spectral purity at 404.7 nm, may provide substantial enhancement of this laser's performance. The suggested use of N_2^{15} may prove useful as well. Whatever the potential applications of this laser may be, it is hoped that this work will be a useful guide to continue development of this laser.

APPENDIX A

CALCULATION OF EFFECTIVE ABSORPTION COEFFICIENTS

When performing absorption calculations in gases, it is frequently useful to have an estimate of the absorption coefficient when using broadened sources. It is clear that Beer's law holds for sources which are very narrow compared to the absorption line. When the source is much broader than the absorption line, the analysis is also straightforward [see for example, Mitchell and Zemansky (Ref. 19 in Chapter I), p. 116 et seq.]. For the mercury laser, the pumping lamp emission line and the laser medium absorption line have comparable widths. A simple approximation will be found which is useful for this case.

Consider a doppler broadened absorption line with width $\Delta\nu_D$ (FWHM), pumped by a source with width $\alpha\Delta\nu_D$. Then the fractional intensity transmitted through an absorption length ρ is given by

$$T = \frac{\int_{-\infty}^{\infty} e^{-(\omega/\alpha)^2} e^{-k_0\rho e^{-\omega^2}} d\omega}{\int_{-\infty}^{\infty} e^{-(\omega/\alpha)^2} d\omega} \qquad (A.1)$$

where $\omega = \sqrt{4\ln(2)}\ (\nu - \nu_0)/\Delta\nu_D$, and k_0 is the absorption coefficient at line center,

$$k_0 = \frac{2}{\Delta\nu_D}\sqrt{\frac{\ln 2}{\pi}}\ \frac{\lambda^2}{8\pi}\ \frac{g_2}{g_1}\ \frac{N}{\tau} \qquad (A.2)$$

In this expression λ is the wavelength of the transition, g_2 and g_1 are upper and lower level degeneracies, N is the atomic density, and τ is the radiative lifetime of the upper level.

The right hand side of Eq. (A.1) is easily integrated to yield

$$T = \sum_{n=0}^{\infty} (-1)^n\ \frac{(k_0\rho)^n}{n!\sqrt{1+n\alpha^2}} \qquad (A.3)$$

An effective absorption coefficient k_{eff} can be defined by assuming that the incident radiation is absorbed as

$$I(x) = I_0\, e^{-k_{eff}x}$$

and then

$$T = e^{-k_{eff}x}$$

hence

$$k_{eff} = -\frac{\partial T}{\partial \rho}\Big/ T$$

or

$$k_{eff} = k_0 \frac{\sum_{n=0}^{\infty} (-1)^n \frac{(k_0\rho)^n}{n! \sqrt{1+(n+1)\alpha^2}}}{\sum_{n=0}^{\infty} (-1)^n \frac{(k_0\rho)^n}{n! \sqrt{1+n\alpha^2}}} \qquad (A.4)$$

If the absorption parameter $k_0\rho \ll 1$, only the first term in the expansion is important and we get

$$k_{eff} = \frac{k_0}{\sqrt{1+\alpha^2}} \qquad (A.5)$$

Numerical calculations have shown this to be a useful approximation over wide ranges of $k_0\rho$ if $\alpha \leq 1$. The accuracy improves, as expected, as α approaches zero. The maximum error is $< 10\%$ for $\alpha = 1$. For precise calculation Eq. (A.3) should still be used, but this approximation has proven very useful for mercury laser calculations, since we expect $\alpha \leq 1$ in our pumping schemes.

If we assume $\alpha = 1$, the value of k_{eff} for the 253.7 nm line is $\sim 4.6 \cdot 10^{-13}$ cm^2, corresponding to an absorption depth of ~ 200 μ when the mercury density is 10^{14} cm^{-3}.

APPENDIX B

LASER GYRO APPLICATIONS

The mercury vapor laser has some unique properties which may particularly suit it to laser gyro applications. The laser tube itself is a passive absorption cell, and contains no discharge. Thus, cataphoretic effects which contribute to a null shift are absent. Also, the gain in a carefully processed sealed-off laser tube should not change appreciably over time, since there exist no gas cleanup mechanisms associated with a discharge. There are no electrodes to fail, a common problem in gas discharge lasers. Since the excitation source is external to the laser medium, the optical pumping lamps may be replaceable in the field. Finally, the somewhat shorter wavelength would make a mercury laser gyro slightly more rotationally sensitive than the commonly used He-Ne laser gyro.

Since the multi-oscillator approach to laser gyro design is of such current interest, we will discuss the application of the Hg laser for this approach. We will consider the case in which the laser is to be operated containing a 50-50 mixture of Hg isotopes. In this case, the isotope shift in frequency on the laser transition between the two isotopes is used to generate the bias required to minimize lock-in problems.

One possibility would be to select two Hg isotopes which have a large enough isotopic shift at 546.1 nm that their gain profiles do not overlap

in frequency. This will reduce isotopic competition and lock-in problems. From inspection of Fig. 5(c), Chapter I, the most likely candidates for this approach are Hg^{198} and Hg^{204}. Their frequency difference on the laser transition is 2.52 GHz. Using Hg^{196} and Hg^{204} may be an even better choice, but no data is available for the shift of Hg^{196} at 546.1 nm.

Since the pumping on the 253.7 nm line is isotope specific, the pump lamps must also contain a 50-50 mixture of the chosen isotopes. This will have the effect of reducing the pumping intensity by 1/2 for each pump line for each isotope. To avoid a consequent four-fold reduction in gain, two pumping lamps should be used. The use of two pumping lamps arrayed in a symmetrical manner about the laser medium will also give a more uniform pumping distribution in the tube than in our experiments.

Careful attention must be paid to the optical pumping geometry. It may prove impractical to use a double-elliptical pump cavity in an Hg laser gyro. A potentially useful technique would be to use a coated diffuse reflector surrounding the laser tube and pumping lamps. A coating of $BaSO_4$ is the first choice for this purpose. It has a high reflectivity for both pump lines, and should not be degraded by the intense ultraviolet pumping radiation. It is also readily available commercially. Whether in powder form or in some form of baked-on coating, the $BaSO_4$ particles should be densely packed. In a loosely packed powder the individual grains may have high reflectivity, but the light tends to become trapped by reflection into interstices deep in the powder.

With proper care in laser tube processing and optimization of the optical pumping lamps and geometry, it should prove possible to make a reasonably compact Hg laser gyro. However, there is one serious disadvantage to

this system, the sensitivity of the device to the ambient temperature. A laser filled with a 50-50 isotopic mixture in a 3 mm bore tube will have to be operated at over 40° C to achieve optimum gain. Thus, if rapid start-up of the laser is required, some sort of stand-by power will be needed to maintain the Hg density near its optimum value. Only further study will show whether the many potential advantages of the Hg laser in gyro applications will outweigh this disadvantage.

REFERENCES

CHAPTER I

1. R. W. Wood, Phil. Mag. 50, 774 (1925).
2. E. Gaviola, Phys. Rev. 34, 1373 (1929).
3. E. Gaviola, Phys. Rev. 35, 1226 (1930).
4. E. W. Samson, Phys. Rev. 40, 940 (1932).
5. H. Klumb and P. Pringsheim, Z. Physik 53, 610 (1928).
6. N. Djeu and R. Burnham, Appl. Phys. Letters 25, 350 (1974).
7. G. H. Kimbell and D. J. Leroy, Can. J. Chem. 38, 1714 (1960).
8. J. A. Berberet and K. C. Clark, Phys. Rev. 100, 506 (1955).
9. Z. Ben-Lakhdar-Akrout, J. Butaux, and R. Lennuier, J. de Physique 36, 625 (1975).
10. A. Yariv, Quantum Electronics, Wiley, 1967.
11. T. Holstein, Phys. Rev. 72, 1212 (1947); Phys. Rev. 83, 1159 (1951).
12. G. C. King and A. Adams, J. Phys. B 7, 1712 (1974).
13. J. Pitre, K. Hammond, and L. Krause, Phys. Rev. A 6, 2101 (1972).
14. J. P. Barrat, J. L. Cohan, and Y. Lecluse, C.R. Acad. Sci. B 262, 609 (1966).
15. R. Burnham and N. Djeu, J. Chem. Phys. 61, 5158 (1974).

16. P. Jean, M. Martin, J. P. Barrat, and J. L. Cohan, C.R. Acad. Sci. B 264, 1709 (1967).

17. A. B. Callear and R. G. W. Norrish, Proc. Roy Soc. A 266, 299 (1962).

18. Y. B. Golubovskii and R. I. Lyagushchenko, Opt. and Spectrosc. 40, 124 (1976).

19. A. C. G. Mitchell and M. W. Zemansky, Resonance Radiation and Excited Atoms, Cambridge Univ. Press, 1934.

20. D. Vienne-Casalta and J. P. Barrat, J. de Physique 36, 367 (1975).

21. D. Alpert, A. O. McCoubrey, and T. Holstein, Phys. Rev. 76, 1257 (1949).

22. H. Schuler and E. G. Jones, Z. Phys. 74, 631 (1932).

REFERENCES

CHAPTER II

1. Max Artusy, Neil Holmes, and A. E. Siegman, Appl. Phys. Lett. 28, 133 (1976).
2. Max Artusy, Ph.D. thesis, Stanford University, 1977.
3. P. Jean, M. Martin, J. P. Barrat, and J. L. Cohan, C. R. Acad. Sci. B 264, 1791 (1967).
4. R. Burnham and N. Djeu, J. Chem. Phys. 61, 5158 (1974).
5. Z. Ben-Lakhdar-Akrout, J. Butaux, and R. Lennuier, J. de Physique 36, 625 (1975).
6. A. B. Callear and R. G. W. Norrish, Proc. Roy. Soc. A 266, 299 (1961).
7. D. Vienne-Casalta and J. P. Barrat, J. de Physique 36, 367 (1975).
8. R. W. Wood and E. Gaviola, Phil. Mag. 6, 271 (1928).
9. C. K. Rhodes, private communication.
10. L. Krause, USAF Technical Report AFAL-TR-73-342, 1973.